Aalto University School of Science and Technology
Inorganic Chemistry Publication Series
Espoo 2010 No. 9

CATION ORDERING AND OXYGEN STOICHIOMETRY IN DOUBLE PEROVSKITE SYSTEMS, $(Sr,La)_2FeTaO_{6-\delta}$ AND $LaBaCo_2O_{5+\delta}$

Doctoral Dissertation

Eeva-Leena Rautama

Dissertation for the degree of Doctor of Science in Technology to be presented with due permission of the Faculty of Chemistry and Materials Sciences for public examination and debate in Auditorium KE 2 at Aalto University School of Science and Technology (Espoo, Finland) on the 16th of July, 2010, at 12 noon.

Aalto University
School of Science and Technology
Faculty of Chemistry and Materials Sciences
Department of Chemistry

Aalto-yliopisto
Teknillinen korkeakoulu
Kemian ja materiaalitieteiden tiedekunta
Kemian laitos

Supervisor:

Prof. Maarit Karppinen
Laboratory of Inorganic Chemistry
Aalto University School of Science and Technology

Pre-examiners:

Prof. Tor Grande
Department of Materials Science and Engineering
Norwegian University of Science and Technology

Dr. Valery Petrykin
J. Heyrovsky Institute of Physical Chemistry
Academy of Sciences of Czech Republic

Opponent:

Prof. J. Paul Attfield
School of Chemistry
The University of Edinburgh

Aalto University

Author Eeva-Leena Rautama

Name of the dissertation
Cation Ordering and Oxygen Stoichiometry in Double Perovskite Systems, $(Sr,La)_2FeTaO_{6-\delta}$ and $LaBaCo_2O_{5+\delta}$

Manuscript submitted 30.4.2010	Manuscript revised N/A

Date of the defence   16.7.2010

☐ Monograph	☒ Article dissertation (summary + original articles)

Faculty   Faculty of Chemistry and Materials Science

Department   Department of Chemistry

Field of research Inorganic Chemistry

Opponent(s)   Prof. J. Paul Attfield

Supervisor   Acad. Prof. Maarit Karppinen

Instructor

The present thesis consists of five publications, reviewed with relevant literature data. Different types of double perovskites were investigated and consequently, two new compounds are introduced accompanied by their extensive characterization.

The B-site ordered double perovskite $(Sr_{1-x}La_x)_2FeTaO_6$ (x = 0..0.3) achieved by R^{III}-for-Sr^{II} substitution is described by its synthesis, crystallographic features and physical properties. The degree of order of Fe and Ta cations is determined from the X-ray diffraction data after determining the crystal structure. The degree of order is achieved to a practically full extent in the highest-doped samples with respect to the disordered parent phase. The decrease in the Fe oxidation state and its local coordination is analyzed by ^{57}Fe Mössbauer spectroscopy and Fe and Ta L-edge XANES spectroscopy, combined with wet-chemical analysis. The physical properties are found to be similar to those of the disordered parent phase, indicating paramagnetism at room temperature with insulating behavior.

The synthesis of the A-site and oxygen-vacancy ordered $LaBaCo_2O_{5+\delta}$ (δ = 0.5) compound is presented for the first time. The crystal and magnetic structure is determined by neutron diffraction and the microstructure probed by electron diffraction and high-resolution transmission microscopy. The properties resemble the previously known layered cobalt oxides but a partial A-cation and oxygen-vacancy disorder is evidenced. The compound undergoes a spontaneous magnetization at ~320 K which is the highest measured compared to other similar compounds. In addition, a new polymorph of the δ = 1 phase is described. This structure consists of ordered, nanometer-sized domains affecting the crystal lattice and the physical properties. The chemical pressure effect was realized in both A- and B-site ordered perovskites. For the B-site ordered compounds, the band structures of halfmetallic A_2FeMoO_6 (A = Ca, Sr, Ba) were calculated and compared to the literature results. As a main result, a decrease of the partial density of states -comparable to the Fe and Mo valence states- is observed, supporting the reported experimental data. For the A-site ordered compounds, R^{III} cation substitution with precise oxygen engineering in $RBaCo_2O_{5+\delta}$ (δ = 0.5) system is demonstrated. A partial A-cation and oxygen-vacancy order is studied by crystal-chemical features and physical properties. While the disorder has an effect on the unit cell in addition to magnetic and transport properties, oxygen engineering plays a significant role in fine-tuning of the same properties.

Keywords   double perovskite, cation ordering, oxygen ordering, oxygen stoichiometry

Publisher   Department of Chemistry

Print distribution   Laboratory of Inorganic Chemistry, P.O.Box 16100, 00076 Aalto, Finland

☒ The dissertation can be read at http://lib.tkk.fi/Diss/2010/isbn9789526032566

Tekijä   Eeva-Leena Rautama

Väitöskirjan nimi
Kationijärjestäytyminen ja happistoikiometria $(Sr,La)_2FeTaO_{6-\delta}$ ja $LaBaCo_2O_{5+\delta}$ -kaksoisperovskiittirakenteissa

Käsikirjoituksen päivämäärä 30.4.2010	Korjatun käsikirjoituksen päivämäärä

Väitöstilaisuuden ajankohta   16.7.2010

☐ Monografia	☒ Yhdistelmäväitöskirja (yhteenveto + erillisartikkelit)

Tiedekunta   Kemian ja materiaalitieteiden tiedekunta
Laitos   Kemian laitos
Tutkimusala   Epäorgaaninen kemia
Vastaväittäjä(t) Prof. J. Paul Attfield
Työn valvoja   Akat. prof. Maarit Karppinen
Työn ohjaaja

Tässä väitöskirjassa tutkittiin erilaisia kaksoisperovskiitteja ja kaksi uutta yhdistettä syntetisoitiin ja karakterisoitiin kattavasti rakenteensa ja kemiallisten ja fysikaalisten ominaisuuksiensa puolesta.

B-paikan suhteen järjestäytymistä tutkittiin $(Sr_{1-x}La_x)_2FeTaO_6$ ($x = 0..0.3$) –systeemissä. Kahdenarvoisen Sr-kationin osittainen substituutio kolmenarvoisella La:lla mahdollisti Fe ja Ta –kationeiden järjestäytymisen, jolloin normaalisti perovskiittirakenteisesta yhdisteestä muodostui B-paikan suhteen järjestäytynyt kaksoisperovskiitti. Rakenneanalyysi paljasti monokliinisen rakenteen, jossa B-kationeiden järjestäytymisaste kasvoi substituutioasteen mukaisesti päätyen lähes täydelliseen järjestäytymiseen. Raudan keskimääräisen hapetusasteen voitiin osoittaa laskeneen substituution vaikutuksesta Fe ja Ta L-reunojen XANES- ja ^{57}Fe Mössbauer spektroskooppisesti. Näytteiden stoikiometrisuus hapen suhteen osoitettiin kemiallisesti. Yhdisteet järjestäytyvät antiferromagneettisesti matalassa lämpötilassa, joskin Néélin lämpötila nousee hieman substituutioasteen kasvaessa materiaalien pysyessä eristävinä.

A-paikan ja happivakanssien suhteen järjestäytyneen $LaBaCo_2O_{5+\delta}$ ($\delta = 0.5$) –yhdisteen valmistus esiteltiin ensimmäistä kertaa. Yhdisteen kiderakenne ja magneettinen rakenne määritettiin neutronidiffraktiomittausten perusteella laajalla lämpötila-alueella. Elektronidiffraktio yhdistettynä korkean resoluution elektronimikroskopiaan tukivat pulverihavaintojen osittaista vakanssien epäjärjestäytymistä. Yhdisteen magneettiset ominaisuudet muuttuvat huoneenlämpötilan ferrimagnetismista antiferromagneettiseksi jäähdytettäessä kun taas sähkönjohtavuus muuttuu metallisesta eristäväksi lähellä huoneenlämpötilaa. Saman yhdisteen stoikiometrisesta faasista löydettiin uusi järjestäytymisen muoto, joka koostuu nanomittakaavassa järjestäytyneistä kuutiosta, jotka pakkautuvat epäjärjestäytyneeseen perusrakenteeseen mikrorakenteen vaikuttaessa fysikaalisiin ominaisuuksiin.

Vyörakennelaskut spin-polarisoituneille A_2FeMoO_6 (A = Ca, Sr, Ba) –yhdisteille osoittivat Fe:n ja Mo:n sekavalenssitilan muuttuvan teoreettisesti samoin kuin kokeelliset havainnot ovat osoittaneet. Harvinaisella maametallilla substituoitu ja happikontrolloitu $RBaCo_2O_{5+\delta}$ ($\delta = 0.5$) –systeemi osoitti kiderakenteeseen ja fysikaalisiin ominaisuuksiin vaikuttavaa epäjärjestäytymistä ja samalla korosti oikean happistoikiometrian tärkeyttä samoihin ominaisuuksiin.

Asiasanat   kaksoisperovskiitti, kationijärjestäytyminen, happijärjestäytyminen, happistoikiometria

Julkaisija Kemian laitos

Painetun väitöskirjan jakelu Epäorgaanisen kemian laboratorio, PL 16100, 00076 Aalto

☒ Luettavissa verkossa osoitteessa http://lib.tkk.fi/Diss/2010/isbn9789526032566

PREFACE

The work presented in this thesis has been carried out in the Laboratory of Inorganic Chemistry at Aalto University School of Science and Technology (TKK), Materials and Structures Laboratory (Tokyo Institute of Technology) and the Laboratoire de Cristallography et Sciences des Matériaux (CRISMAT; University of Caen) between September 2005 and April 2010.

My most important words of appreciation belong to my everyday friends who easily made me forget all the problems at work by dragging me out to the real world and whose support was all I had when life did not go as planned. I also thank my parents for constant support, in addition to always being ready to move me back and forth when it was, again, time to go.

Helsinki, May 2010

Eeva-Leena Rautama

CONTENTS

LIST OF PUBLICATIONS

I   E.-L. Rautama, T.S. Chan, R.S. Liu, J.M. Chen, H. Yamauchi, M. Karppinen, Electron-doping through La^{III}-for-Sr^{II} Substitution in $(Sr_{1-x}La_x)_2FeTaO_6$: Effects on the Valences and Ordering of the *B*-site Cations Fe and Ta, *J. Solid State Chem.* **179** (2006) 111-116.

II   E.-L. Rautama, J. Lindén, H. Yamauchi, M. Karppinen, Iron Valence in Electron Substituted $(Sr_{1-x}La_x)_2FeTaO_6$ Double Perovskite: ^{57}Fe Mössbauer Spectroscopy Study, *J. Solid State Chem.* **180** (2007) 440-445.

III E.-L. Rautama, Ph. Boullay, A.K. Kundu, V. Caignaert, V. Pralong, M. Karppinen, B. Raveau, Cationic Ordering and Microstructural Effects in the Ferromagnetic Perovskite $La_{0.5}Ba_{0.5}CoO_3$: Impact upon Magnetotransport Properties, *Chem. Mater*. **20** (2008) 2742-2750.

IV   E-L. Rautama, V. Caignaert, Ph. Boullay, A.K. Kundu, V. Pralong, M. Karppinen, C. Ritter, B. Raveau, A New Member of the "112" Family, $LaBaCo_2O_{5.5}$: Synthesis, Structure and Magnetism, *Chem. Mater*. **21** (2009) 102-109.

V   E.-L. Rautama and Maarit Karppinen, *R*-site Varied Series of $RBaCo_2O_{5.5}$ $(R_2Ba_2Co_4O_{11})$ compounds with precisely controlled oxygen content, *J. Solid State Chem.* **183** (2010) 1102-1107.

THE AUTHOR'S CONTRIBUTION

Publications I and II   The author defined the research plan together with co-authors, synthesized the samples and did all the characterizations, excluding the XANES measurements. The results were interpreted together with co-authors. The author had a major role in writing the manuscript.

Publication III   The author defined the research plan together with co-authors, prepared the samples and did the X-ray characterizations and chemical analyses. The author participated in writing the manuscript.

Publication IV   The author defined the research plan together with co-authors, designed and conducted the synthesis, made the X-ray and neutron diffraction measurements and analyses and interpreted the results together with co-authors. The author had a major role in writing the manuscript.

Publication V   The author defined the research plan, carried out all the experiments and interpreted the results. The author had a major role in writing the manuscript.

Espoo 28th April 2010

Prof. Maarit Karppinen

LIST OF ABBREVIATIONS

AFM	Antiferromagnetism
CMR	Colossal magnetoresistance
DSC	Differential scanning calorimetry
DFT	Density functional theory
DOS	Density of states
DP	Double perovskite
ED	Electron diffraction
FC	Field cooling
FLAPW	Full-potential linearized augmented plane-wave
FWHM	Full-width at half maximum, describing the width of a peak
HRTEM	High-resolution transmission electron microscopy
HS	High spin
IS	Isomer shift in Mössbauer spectroscopy
IS	Intermediate spin
LDA	Local density approximation
LS	Low spin
MO	Molecular orbital
N(P)D	Neutron (powder) diffraction
RT	Room temperature
SAED	Selected-area electron diffraction
SOFC	Solid-Oxide Fuel Cell
TCOD	Temperature-controlled oxygen depletion
TG	Thermogravimetry
TMR	Tunneling magnetoresistance
XANES	X-ray absorption near-edge structure
XR(P)D	X-ray (powder) diffraction
ZAP	Zone axis pattern
ZFC	Zero field cooling

LIST OF SYMBOLS

a_p	Lattice parameter of a simple perovskite unit cell
A	Atomic site in perovskite structure/large metal cation (*e.g.* Ca, Sr, Ba)
B	Atomic site in perovskite structure/transition metal cation (*e.g.* Fe, Co)
R	Rare-earth element
δ	Overall oxygen non-stoichiometry *per* formula unit
g_i	Fractional occupancy of a cation i in a crystal structure
S	Bragg-William long-range order parameter/spin quantum number
$\square$	Oxygen vacancy in a crystal structure
E_F	Fermi level
T_C	Curie temperature
T_N	Néel temperature
T_{M-I}	Metal-insulator transition
U	Exchange correlation potential of von Barth-Hedin
H_c	Coercive field
μ_{eff}	Effective paramagnetic moment
χ^{-1}	Reciprocal magnetic susceptibility
θ_p	Weiss temperature
$p(O_2)$	Oxygen partial pressure

1 INTRODUCTION

Perovskites and perovskite-related oxides are known to possess a rich variety of magnetic, electrical, optical and catalytic properties. Depending on the elements, perovskites can present ferromagnetic, antiferromagnetic, diamagnetic and spin-glass properties whilst the conductivity can vary from insulation to superconductivity. More recently, perovskites have gained attention as ionic and mixed conductors for solid-oxide fuel cell (SOFC) applications as electrodes and electrolytes. The origin of the wide interest in transition metal perovskites dates back to the discovery of high-temperature superconductivity in perovskite-related copper oxide in mid the 1980s. The efforts to improve the superconducting properties lead to the discovery of another fascinating phenomenon, colossal magnetoresistance (CMR) and later on, tunnelling magnetoresistance (TMR). In terms of chemistry, all of these materials contain the transition metal involved, Cu, Mn, Co or Fe, in a mixed valence state. Establishing the ways to control the metal oxidation states enables the preparation of new related materials. Common for perovskite oxides is also their ability to absorb and desorb oxygen reversibly. Even though this is one of the phenomena used to modify the metal valence states, it simultaneously makes the perovskites good candidates for oxide ion conductors in intermediate temperature SOFCs and oxygen sensors.

In addition to the interesting properties and potential applications of perovskites, the structural aspects have also offered their own branch of research. Especially in complex perovskites, the local environment and distribution of cations and anions control the properties of the material. As the perovskite units are commonly distorted in different ways, each new compound can act as a challenging target.

1.1   Crystal Structure of Double Perovskite Oxides

The flexibility of the perovskite unit allows various ways to modify the crystal structure. New variants can be derived from the basic perovskite structure ABO_3 by substituting one or both of the A- and B-site cations with other suitable cations. The substituent may be located in the crystal lattice either randomly in the original perovskite structure, or the structure may

become an ordered type in which the cations alternate regularly. In the case of an ordered structure the size of the unit cell changes, setting new demands in terms of crystal structure but also creating new properties for the compound, and such ordered compounds are commonly called double- or complex perovskites. At its simplest, replacing half of the B' cations at the B site with B'' cations, a B-site ordered double perovskite (DP) $A_2B'B''O_6$ is formed. Correspondingly, substituting the A site leads to an A-site ordered DP structure $A'A''B_2O_6$. Several B-site ordered DPs were reported already in late 1950s[1] and early 1960s[2,3]. The first A-site ordered, perovskite-related layered compound was YBaCuFeO$_5$[4]. Later, the isomorphs with different B cations and rare-earth (R) cations were realized[5-9]. While the B-site ordered DPs are typically oxygen stoichiometric, the A-site ordered structures exhibit a large concentration of oxygen vacancies (□), located in the layer of the smallest A cation, and require stability of the B cations for pyramidal coordination. Therefore, the structure is best described as an array of layers following the sequence [$A'O$]-[BO_2]-[$A''O_\delta$]-[BO_2]…, where δ stands for the oxygen non-stoichiometry parameter. Figure 1 presents the structures of double perovskites with cell expansions in respect to a simple perovskite lattice parameter, a_p.
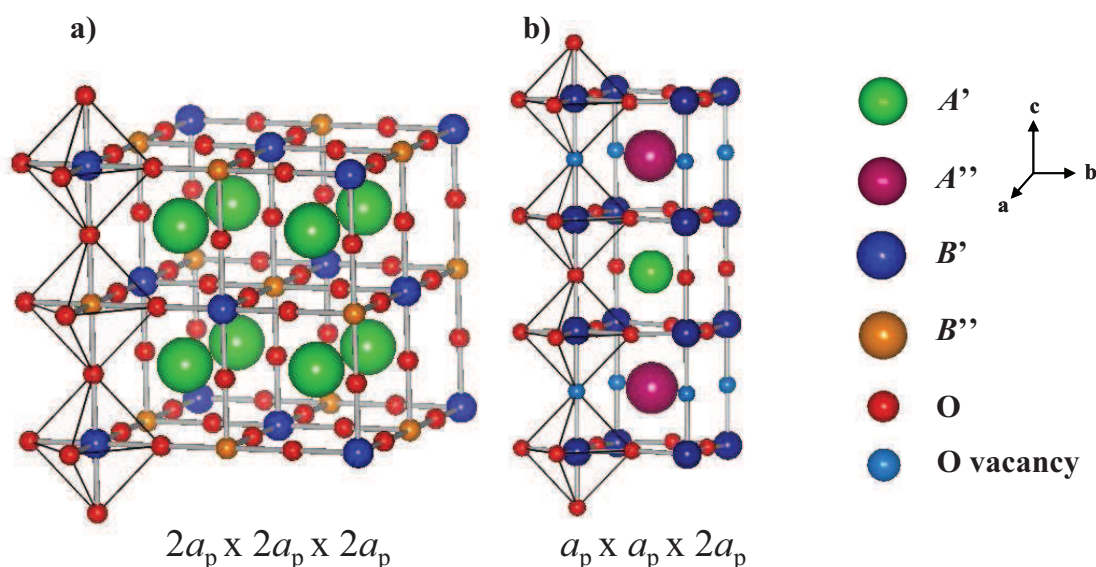
Figure 1. Schematic representations of the a) B-site ordered $A_2B'B''O_6$ and b) A-site ordered $A'A''B_2O_{5+\delta}$ double perovskite structures. The light-blue atoms represent the possible vacant sites in b).

1.2 Role of the Individual Atoms in the Structures

The most characteristic phenomenon of the ordered A_2FeMO$_6$ (M = Mo, Re) and RBaB_2O$_{5+\delta}$ (B = Mn, Co) perovskites is the tendency of the transition metals to exhibit in several mixed-valence states. For all of these compounds, TMR[10] or CMR[11] phenomenon has been observed.[10,9,12-14] The transition metal valence states of A_2FeMoO$_6$ were discussed already in the 1960s[15]. The itinerant d electron of formally pentavalent Mo ($4d^1$; t_{2g}^1) transfers part of its charge and spin density to formally trivalent Fe ($3d^5$; $t_{2g}^3 e_g^2$), and as a consequence the mixed-valence states, Fe$^{II/III}$ and Mo$^{V/VI}$, are realized[16,17]. The precise charge balance between Fe and Mo is then controlled by, $e.g.$ the choice (average size) of the A-site cation constituent.[18,19] The regular arrangement of Fe and Mo atoms, $i.e.$ degree of order, defines the magnetic and transport properties; Sr$_2$FeMoO$_6$ is a good conductor when Fe and Mo atoms are situated practically perfectly but the resistivity increases significantly along with a change in the type of conduction, when the degree of Fe/Mo order is lowered[20]. The hybridization of Fe and Mo t_{2g} states, $i.e.$ valence fluctuation, results in ferro/ferrimagnetic ordering of the material, the saturation magnetization being also the highest for the compound closest to the ideal structure[20]. The valence fluctuation is also supported by band structure calculations where in one spin direction, the Fe and Mo t_{2g} density of states hybridize over the Fermi level (E_F) but in the other direction they are separated by a band gap[10,21]. A total spin imbalance at the E_F causes the carriers to be fully spin-polarized and the materials are referred to as halfmetals[22,23]. When the degree of order in a polycrystalline Sr$_2$FeMoO$_6$ is close to ideal Fe and Mo ordering, the material exhibits TMR effect even above room temperature[10]. Similar behaviour is observed for Ba and Ca variants[24,25] and for B''= Re[13,14] but not for B'' = Nb[26,27], Ta[28] and W[29] as they lack the itinerant $4d$ or $5d$ electrons for the valence fluctuation.

In the A-site ordered RBaB_2O$_{5+\delta}$ (R = trivalent rare-earth cation, B = Mn[30,31], Co[12,32], Fe[33,34]) type of compounds, the transition metal can have mixed valence states of II/III and III/IV if $\delta = 0$ and 1, respectively, or is precisely at III when $\delta = 0.50$. These compounds have been shown to possess several interesting phenomena depending on δ: charge ordering, CMR, metal-insulator transition, structural transitions and several magnetic states on cooling[12,30-34].

All the phenomena are related to the mixed valence states of the transition metals in question. With the case of B = Co the properties are not only determined by the valence state values but

also by the variety of possible spin configurations that can easily overcome each other just by thermal effects. Depending on the structure, the valence states can be controlled either by aliovalent cation substitution or, if the structure allows oxygen vacancies, by varying the oxygen content. The B-site ordered DPs are essentially oxygen stoichiometric such that the access to the valence states of the B cations is through cation substitutions. The A-site ordered DPs typically possess large amounts of oxygen vacancies ($0 \leq \delta \leq 1$), depending on the R constituent, hence tuning the oxygen content is a direct way to achieve the desired transition metal valence states. As a result of the excellent reversibility of oxygen absorption and desorption and oxide ion conductivity the $R\mathrm{BaCo_2O_{5+\delta}}$ phases have been a subject of research as cathodes in intermediate temperature SOFCs[35-39].

1.3 Scope of the Present Thesis

The aim of this work was to design and synthesize new double-perovskite oxides by controlling the ordering of A and B cations and the oxygen vacancy arrangement.

The gradual increase in the B-site cation ordering was studied in the $(\mathrm{Sr_{1-x}La_x})_2\mathrm{FeTaO_6}$ system[I,II]. In order to verify the degree of order, careful analysis by X-ray powder diffraction (XRPD) was conducted. The evolution of the ordering was studied by analyzing the B cation valence states with ^{57}Fe Mössbauer and Fe $L_{2,3}$ and Ta L_3 -edge XANES spectroscopy, and by wet-chemical analyses. The changes in the magnetic properties were also analyzed.

Ordering of the A cations was studied in the $R\mathrm{BaCo_2O_{5+\delta}}$ ($\delta = 0.5$ and 1) system, the main target being in the $R = \mathrm{La}$ compound. A new, microstructurally ordered phase was established using electron diffraction (ED), high-resolution transmission electron microscopy (HRTEM) and XRPD. Its synthesis conditions and properties were considered with respect to the disordered and ordered forms of $\mathrm{LaBaCo_2O_6}$[III]. The $\mathrm{LaBaCo_2O_{5+\delta}}$ ($\delta = 0.5$) phase had not been reported earlier and its crystal and magnetic structures were examined by X-ray and neutron powder diffraction (NPD), ED and HRTEM[IV]. Magnetic and transport properties were determined for all the materials[III,IV].

Chemical pressure effect was studied for both the *A*- and *B*-site ordered double perovskites in two systems. The conduction band was studied by electronic band structure calculations for the *B*-site ordered A_2FeMoO_6 (A = Ca, Sr, Ba) and compared with the experimental results. The R^{III}-cation varied $RBaCo_2O_{5+\delta}$ (δ = 0.5; R = Y, Ho-Sm, Nd, Pr, La) series with precisely adjusted oxygen content was synthesized. The chemical pressure effects on the lattice behaviour, Co valence and physical transitions were realized[V].

2 STRUCTURAL ANALYSIS

Perovskites are known to possess a large variation of distortions that compensate for the demanding ideal cubic structure. Usually the ideal structure is found only in compounds stabilized by an oversized *A* cation (*e.g.* Ba)[40]. Besides the size, a more electronegative *A* cation usually lowers the symmetry[50]. Distorted structures can be interesting just from the structural point of view but more importantly, they affect the physical properties of the compounds. The distortion mechanisms can be divided into three different types: distortions of the octahedra, cation displacements within the octahedra, and tilting of the octahedra[40]. Electronic instability of the *B* cation is the driving force for the first two mechanisms, such as a Jahn-Teller active ion in the structure,[40,41] but the most commonly occurring distortion is the octahedral tilting. It can be understood by tilting inflexible octahedra in separate layers so that the *A*-O bond distance is optimized by becoming shorter but the BO_6 octahedra remain unchanged, preserving their corner-sharing connectivity. The structural changes in the octahedral tilting are small, hence also lowest in energy thus explaining its prevalence[40]. In the case of DPs, the same distortion mechanisms apply but the number of possible resultant space groups is much more limited due to symmetry rules[42,43].

2.1 Powder Diffraction Techniques

The most important methods for studying the degree of order in the DPs among other crystallographic features are X-ray and neutron diffraction. The interpretation of the

diffraction patterns and determination of individual site occupancies in the structural model enables the calculation of the Bragg-Williams long-range order parameter[44] defined as:

$$S = 2g_i-1, \tag{1}$$

where g_i stands for the occupancy of the cation i at its correct crystallographic site.

If the atomic numbers of the cations under interest differ enough, the fractional occupancies can be extracted already from the X-ray diffraction data. This is often valid with the B-site ordered DP oxides due to the nature of the B site ordering whereas the A-site ordered compounds often involve cations that are distinguishable only by neutron diffraction (Large R^{III}/Ba) as well as the precise location of a light element, such as oxygen. As neutrons are scattered by the nuclei, there is no linear dependency on the atomic number in either the scattering factors or the diffraction angle, allowing many features to be analyzed even for the lightest elements. In addition, the interaction of the neutron magnetic moment with magnetic atoms in the target material provides information on the magnetic structure. Occasionally it happens that some nuclei scatter relatively better by X-rays than neutrons, therefore the best way is to combine XRPD and NPD data simultaneously. The X-ray scattering factors and neutron scattering lengths for the elements relevant to the present work are collected in Table 1. The $f(0)$ were calculated from the Cromer-Mann coefficients of the investigated ions.

Table 1. X-ray scattering factors for defined ions and neutron scattering lengths for the atoms used in this work[45].

Element (charge)	Fe (II/III)	Ta (V)	O (-II)	La (III)	Ba (II)	Co (III)
X-ray scattering factor, $f(0)$	23.67/22.71	66.89	8.40	52.27	50.98	24.39
Neutron scattering length [fm]	-	-	5.80	8.24	5.07	2.49

The present NPD data were collected with high-resolution instrument D2B at the Institute Laue-Langevin (ILL) in Grenoble, France.

The Rietveld method[46,47] is an important technique to obtain more detailed information on the crystal structures from powder diffraction patterns. The whole diffraction pattern is calculated based on a structural model and compared to an experimental one. In the refinement, instrumental-related factors are taken into account along with the crystallographic model and

compared to each other point by point. The parameters defining the diffraction profile are refined and the residual sum is minimized by the least-square method. The Rietveld refinement is also applicable for magnetic structures as, in addition to the cell information, the absolute value and the direction of the moment of each magnetic atom can be obtained. Limitations are attributed to the nature of powder diffraction; there are usually only a few Bragg reflections originating from the magnetic cell and they are often weak.

If the structural model for the Rietveld refinement is not available beforehand, other ways to construct a structural model are needed. In this work, computational indexing and other methods provided by the FullProf Suite[45] and Structure Prediction Diagnostic Software (SPuDS)[48] were used.

2.2 Electron Diffraction and High-resolution Transmission Electron Microscopy

In the present work, ED and HRTEM observations were closely combined with the XRD and NPD data of $LaBaCo_2O_{5+\delta}$ compounds to ensure the validity of the analysis and to study the crystallographic fine structure in each case. When ED is performed for small crystals of a powder sample, it very often happens that the crystals are nonhomogenous and/or present twinning, making a straightforward interpretation of the three diffraction methods sometimes difficult. Despite this, important details can be established.

3 CONTROL OF CATION ORDERING

Perovskite oxides tend to exhibit ordering of either (or both) A and B cations if the constituents are suitable. This means that the cations should differ enough in terms of charge, size and/or preferred coordination sphere.

In B-site ordered double perovskites, the B cations are ideally situated in an octahedral, corner-sharing coordination sphere as in a simple perovskite, and the degree of order is

mainly controlled by the difference in charge and ionic radius of the B cations. The bigger the charge difference, the higher is the degree of order at the B site. When the charge difference is larger than two, as with $A^{II}_2B'^{II}B''^{VI}O_6$ (*e.g.* Sr_2FeWO_6[29]) and $A^{II}_2B'^{I}B''^{VII}O_6$ (*e.g.* Sr_2NaReO_6[2], Sr_2LiOsO_6[49]) compounds, complete ordering is usually achieved. If the charge difference is precisely two, *i.e.* $A^{II}_2B'^{III}B''^{V}O_6$, various degrees of order are observed, depending on the individual B cations and the synthesis techniques employed, but also on the particular A cation in a manner that the highest ordering is achieved with the smallest A constituent[40,50].

The ordering about A cations is less typical and can be divided into several categories: $(A,\square)BO_3$,[51] $A'A''B_2O_{5+\delta}$[4,12,32], $A'A''_2B_3O_{6+\delta}$[52,53] and $A'A''_3B_4O_{12}$.[54-58] In the first type the cation vacancies order but the structure still preserves a simple perovskite unit cell. The second type is an example of a layered structure with high oxygen deficiency, which consists of altering layers of $A'O$ and $A''O_\delta$, doubling the unit along the c direction. The typical nature of this structure is that the anion vacancies also order when $\delta > 0$, thus effecting on the unit cell multiplication mainly in the b direction but also along the a and c axes. The unit cell expansion is dependent on the particular A and δ parameters and for this structure, the B cations do not have to be equal. The layered structure is not limited to two different AO layers as observed with $A'A''_2B_3O_{6+\delta}$ compounds but their amount can be increased by varying the A cation ratio[52], the simplest example being the triple layer perovskite $YBa_2Cu_3O_{6+\delta}$[52]. The $A'A''_3B_4O_{12}$ formula is an example of A-site ordering in both a and b directions and it requires ultra-high pressures to form.

In addition, there exist a few compounds of the type $A'A''B'B''O_6$ that display both A- and B-site cation ordering[59,60].

3.1 Role of Oxygen Partial Pressure

Conditions under low oxygen partial pressure are crucial in the synthesis of materials which do not prefer ordering in either A or B-site perovskites. When dealing with cation ordering about A or B, low $p(O_2)$ is needed to stabilize the low valence states during the structure

formation as observed for the *B*-site ordered Sr_2FeMoO_6[61]. In the case of *A*-site ordering in structures which can occur in both disordered and ordered forms and when the former is favored, low $p(O_2)$ is also the key. Mainly this involves *A* cations whose ionic radii are too similar to support ordering, as is with La^{III} and Ba^{II}. In this case, low $p(O_2)$ is needed to force the La^{III} to take an eight-fold coordination instead of the more common 12-fold for the larger Rs[30,62,63]. This results in the separated *R* layer having a high amount of oxygen vacancies. In the case of *B* = Mn, a reductive atmosphere is required in addition to prevent the stable Mn^{IV} oxidation state that forms more stable structures, such as $BaMnO_{3-\delta}$[30]. In fact, the low $p(O_2)$ in this case is needed for each *R* constituent[30,64,65]. The *B* = Fe requires as strict synthesis conditions[78] and for this phase there is so far no details of the *R* = La compound.

The fully oxygenated structures are achieved by low-temperature (~300 °C) O_2 annealings[30,63,66]. Treatments at higher temperatures allowing cation movement will destroy the layered ordering again. Materials synthesized under reduced oxygen partial pressures typically demonstrate a rapid incorporation with oxygen in a single step at a narrow temperature range[30,**III,IV**] and therefore the intermediate stoichiometries are gained best by back reduction or temperature-controlled oxygen depletion (TCOD)[67].

In addition to disordered and ordered phases, $LaBaCo_2O_{5+\delta}$ can also facilitate ordering on the microstructural scale when the $p(O_2)$ is varied[**III**].

3.2 *B* site Ordering in $A_2Fe^{III}B^VO_6$ Double Perovskites

The iron-containing $A_2Fe^{III}B^VO_6$ type of compounds present both *B*-site ordered and disordered systems. When *B* = Mo, ordering up to *S* = 0.96 can be achieved between nominally trivalent Fe and pentavalent Mo due to the valence mixing between these cations[68]. In contrast, the nonmagnetic pentavalent *B* = Nb[27,69] and Ta[28] do not order with Fe^{III} except for a minor effect (less than *S* = 0.10) when high-enough synthesis temperature is employed[70,**I**] thus their formulas are more informatively written as single perovskite $A(Fe_{0.5}B_{0.5})O_3$. If a compound is not prone to intrinsic electron doping but possesses ordered structure, the explanation usually lies in the adequate size difference between the *B* cations as observed in A_2FeSbO_6[27,71] and A_2FeBiO_6[72,73]. The Nb^V and Ta^V have octahedral ionic radii of

0.64 Å compared to 0.645 Å of a high-spin Fe^{III} whereas $r(Bi^V)$ and $r(Sb^V)$ are 0.60 Å and 0.76 Å, respectively[74]. Even though the size difference between Fe and Sb is not very significant, empirically it has been observed that the B = Sb compounds have a higher degree of order than those of Nb and Ta[50]. The compounds with Nb^V, Ta^V, Sb^V and Bi^V, ordered or not, are antiferromagnetic insulators with unoccupied outer d orbitals. However, $Sr_2FeVO_{5.4}$ is ferrimagnetic with high oxygen-deficiency as the vanadinium is in various valence states without an ordered structure[75,76].

The actual ordering process in the B-site DPs is empirically shown to be kinetically controlled over a wide temperature range. This is evidenced by the increase in ordering with increasing temperature which was seen in two case studies for different materials[50,77] and in some individual studies[70,II]. After a certain temperature point the ordering starts to decrease which points to an increase of entropy and the system turning into a thermodynamically controlled one. In total, this would suggest that the highest degree of order is obtained at fairly low temperature with long synthesis time[20]. In practice, high temperatures are often used for enhancing the sluggish cation movement.

3.3 A-site Ordering in $RBaB_2O_{5+\delta}$ Double Perovskites

The ordering process in the A-site ordered compounds differs from the B-site ordered DPs and is more controlled by cation size difference and preferred coordination tendency of the A cations than by their charge difference. Large interest has been paid towards $RBaB_2O_{5+\delta}$ phases with B = Co, Fe or Mn. For these compounds, the oxygen non-stoichiometry parameter can vary from δ = 0 to 1, depending on the R and B constituents. $RBaCo_2O_{5+\delta}$ and $RBaFe_2O_{5+\delta}$ behave rather similarly, that is, δ increases in a manner that the maximum δ is obtained with the largest possible R as the A cation and with the smallest R cations, the maximum δ value is practically $0.5^{12,32,78}$. The oxygen amount in the R layer is related to the coordination chemistry of the rare-earth cations that varies along their size from CN = 8 to 12. In contrast, Ba as a large cation stabilizes for CN = 12 in perovskite-related structures and this explains why the vacancies are located in the R layer instead of the BaO layer.

Considering the chemical pressure effect in the RBaCo$_2$O$_{5+\delta}$ family by substituting the R cation with larger equivalents, starting from the first reported parent phase YBaCo$_2$O$_{5+\delta}$[6], the coordination effect is very nicely seen. Trivalent Y and Ho are the smallest rare-earth cations that allow the structure to be formed and order readily with the significantly larger Ba^{II} cation. Layers of YO$_\delta$ and BaO in an ordered manner are obtained rather easily when compared to the synthesis of larger rare earths, *i.e.* short synthesis time in simplest atmosphere (air) is enough. Yttrium favors the small coordination number (CN = 8) and the structure tends to form as YBaCo$_2$O$_{5.0}$ (δ = 0). Coordination number 10 can also be stabilized for Y, and therefore with intensive oxidation, also the δ = 0.5 stoichiometry is obtainable. As the size of the R^{III} cation increases, CN = 10 becomes more stable and DPs with the intermediate Rs ((Tb)-Sm) form the easiest with the stoichiometry close to δ = 0.5 and CN = 8 (δ = 0) is also possible for these compounds when treated properly. The 12-fold coordination is not favored and therefore the highest obtained δ is about 0.65 with R = Sm. Increasing the R^{III} size up to the largest Rs (Nd, Pr, La), CN = 12 starts to dominate and the stoichiometric double perovskites (δ = 1) are reported for NdBaCo$_2$O$_{5+\delta}$ and LaBaCo$_2$O$_{5+\delta}$ by chemical oxidation[79] and under elevated O$_2$ pressure[63,III], respectively. The intermediate stoichiometry δ = 0.5 (CN = 10) is still easily obtainable with appropriate treatments but to reach the oxygen-depleted structure is more difficult than with the small or intermediate Rs. For the largest R = La, this has proven to be extremely tricky but is still somewhat possible. In fact, recently it was shown that even a lower value than δ = 0 is obtainable by a chemical reductant method[80].

Nevertheless, the stability of the higher oxidation states of the B cation matters as well: RBaMn$_2$O$_{5+\delta}$ does not share the limits in the maximum δ as Mn^{IV} is more stable compared to Fe^{IV} and Co^{IV}. Hence it can be concluded that the structure formation is not solely dependent on the R cation coordination chemistry but also transition metal oxidation states act as a force for the resultant structure.

The degree of order of the A-site cations, or RO$_\delta$ and BaO layers, has not been a target for intensive investigation. This is because one can assume perfect ordering of the small and intermediate Rs with Ba^{II} cation as its size and coordination preferences are different enough. Only with Rs that favor CN = 12 together with Ba, this may be worth to consider. In addition, the RBaCo$_2$O$_{5+\delta}$ system is more complicated as the oxygen vacancy ordering (discussed in the

following chapter) also plays a role in the structure formation. Recently, there have been reports on partial oxygen vacancy disorder and resulting substructures[81,IV] with R = Pr and La compounds that also affect the physical properties.

3.3.1 Oxygen Vacancy Ordering

Oxygen vacancy ordering comes into question with the RBaB_2O$_{5+\delta}$ structure of $\delta > 0$ stoichiometry, highlighting the $\delta = 0.5$ stoichiometry. The importance of establishing the correct oxygen vacancy ordering and resultant superstructure is its role in the physical properties and magnetic structure determination.

The most intensively studied are the B = Co phases as they have shown various possible structures depending on δ and R. While the excess oxygen in respect to the RBaCo$_2$O$_{5+\delta}$ phase orders, the unit cell is multiplied in different manners. At its simplest, the unit cell doubles along b axis in addition to stacking along c axis (a_p x $2a_p$ x $2a_p$ doubling) but other stable structures have been observed with different unit cell multiplicities. For YBaCo$_2$O$_{5+\delta}$, two superstructures are found: tetragonal $3a_p$ x $3a_p$ x $2a_p$ (332) that results in a composition of δ = 0.44 and orthorhombic a_p x $2a_p$ x $2a_p$ (122) with $\delta = 0.5$[6,32]. The vacancy ordering leading to 122-type doubling in *Pmmm* symmetry with $\delta = 0.5$ has been considered for the whole series with varying R but recently, symmetry analyses combined with single crystal studies have revealed that at least for the smallest R constituents (Y, Ho, Dy) the correct doubling is of $2a_p$ x $2a_p$ x $2a_p$ (222) type in an orthorhombic *Pmma* symmetry[82,83]. In addition, for HoBaCo$_2$O$_{5+\delta}$ with $\delta = 0.3$, an ordering with $3a_p$ x $3a_p$ x $2a_p$ (332) superstructure has been evidenced[24,84]. Above $\delta = 0.5$, at least PrBaCo$_2$O$_{5+\delta}$ ($\delta = 0.75$) has shown a stable $2a_p$ x $2a_p$ x $2a_p$ (222) doubling in respect to a tetragonal *P4/mmm* symmetry. Figure 2 presents the most typical superstructures observed for the B = Co phases.

Pmma ($2a_p$ x $2a_p$ x $2a_p$), $\delta = 0.50$; R = Y, Ho, Dy   *Pmmm* (a_p x $2a_p$ x $2a_p$), $\delta = 0.50$

P4/mmm ($3a_p$ x $3a_p$ x $2a_p$), $\delta = 0.44$; R = Y   *P4/mmm* ($2a_p$ x $2a_p$ x $2a_p$), $\delta = 0.75$; R = Pr
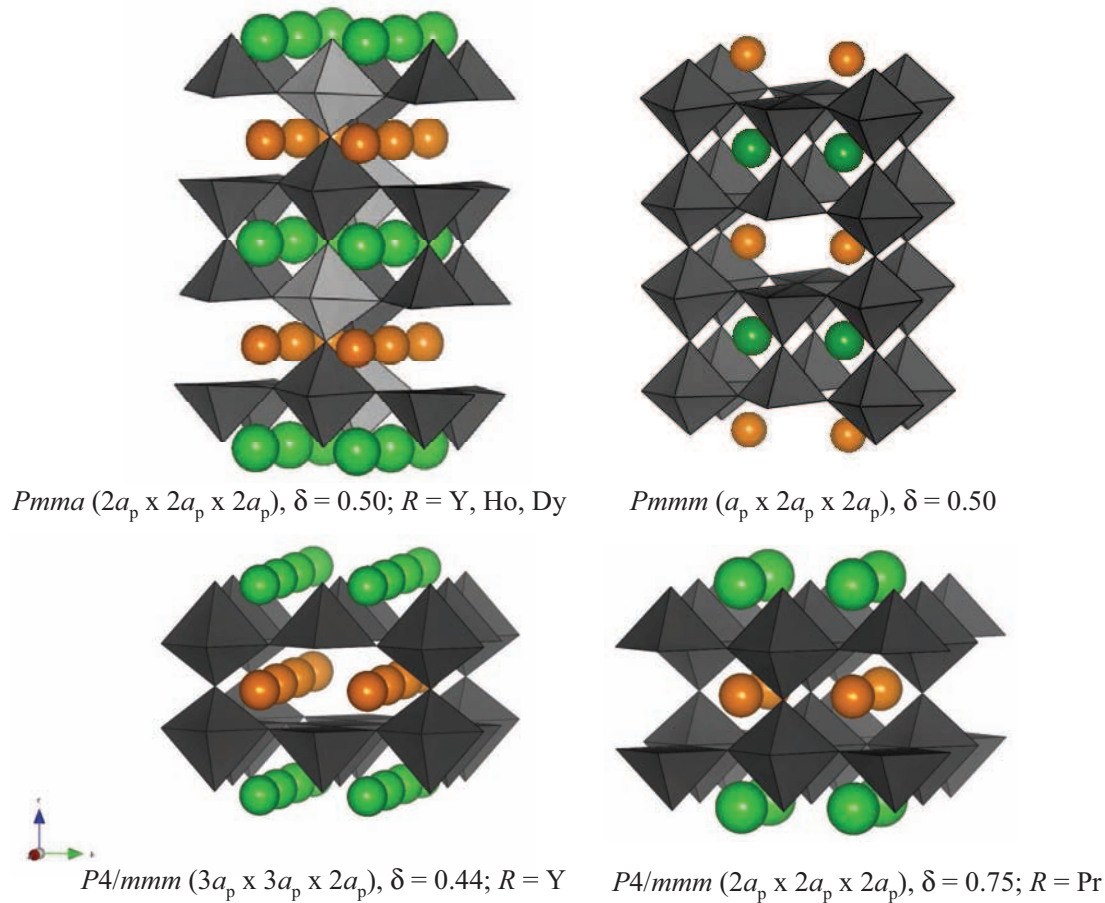
Figure 2. Typical superstructures observed for RBaCo$_2$O$_{5+\delta}$ phases. The structures are adapted from References [12,81,83].

Overall, the oxygen vacancy ordering has a strong effect on the resulting structure. With RBaCo$_2$O$_{5+\delta}$ compounds, the δ-dependent superstructures are changeable, usually reversibly so and are controlled by the oxygen partial pressure in the surrounding atmosphere, either during the synthesis or by post-annealing. All the R variants can be brought to at least the $\delta = 0.5$ stoichiometry that has gained the main interest among these compounds. In addition to the $p(O_2)$ effect and the average oxygen content, the oxygen ordering homogeneity has to be considered. With small Rs, the after treatments for the $\delta = 0.5$ composition are performed either in O$_2$ or air as the as-synthesized samples are typically lacking oxygen. A thermodynamic study by Frontera *et al.*[81] has shown that the stabilization is reached fast under O$_2$ and air but under Ar or N$_2$, needed for annealing of R = Gd-Sm, Nd, Pr and La, the equilibrium state requires significantly more time. A general way to assure desired vacancy order under low $p(O_2)$ is to cool materials extremely slowly after a sufficient treatment period but limitations in homogeneity are often observed[81,**IV,V**]. An elegant way to improve the

vacancy ordering is post treatment in a sealed glass ampoule packed with an external oxygen partial pressure controller (either an oxygen getter or oxygen source)[85,86]. As the average oxygen content does not provide information on the degree of vacancy order, neutron diffraction is needed for the analysis. X-ray diffraction, however, often provides indicative results if the Bragg reflections are carefully examined by their shape and width.

The oxygen vacancy ordering in RBaMn$_2$O$_{5+\delta}$ ($\delta = 0.5$) has been studied for $R = $ La[87], Tb[88] and Y[66,89] phases. The $R = $ La compound was found to crystallize in $Ammm$ space group with a_p x $2a_p$ x $4a_p$ (124) doubling. This means that the manganese octahedra and pyramids alternate along the b axis but along c axis, one polyhedral row obeys a sequence of MnO$_5$-MnO$_6$-MnO$_6$-MnO$_5$ while the other of MnO$_6$-MnO$_5$-MnO$_5$-MnO$_6$. The same pattern is adopted with the $R = $ Y phase but the smaller rare-earth cation gives rise to a $2a_p$ x $2a_p$ x $4a_p$ (224) superstructure in an $Icma$ symmetry[89]. For $R = $ Tb, single phase of TbBaMn$_2$O$_{5+\delta}$ ($\delta = $ 0.5) was not observed but instead the material consisted of almost equal mixtures of $\delta = 0$ and 0.5, the latter having the same superstructure as found for $R = $ Y[88].

In the present thesis, a portion of the LaBaMn$_2$O$_{5+\delta}$ ($\delta = 0.5$), 124-type structure was found in the LaBaCo$_2$O$_{5+\delta}$ ($\delta = 0.5$) compound with a $Cmmm$ $4a_p$ x $2a_p$ x a_p structure, otherwise consisting of $Pmmm$ a_p x $2a_p$ x $2a_p$ doubling[IV].

4 CONTROL OF B CATION VALENCE STATES AND OXYGEN STOICHIOMETRY

The means of controlling the transition metal valence states are different for the B- and A-site ordered double perovskites. The B-site ordered DPs are most often oxygen stoichiometric and the B cations located in octahedral coordination whereas in the layered compounds, the B cations can adopt both pyramidal and octahedral surroundings with various ratios. The valence states of the B cations are best controlled by aliovalent substitution at the A site (or B site if a particular cation is exchangeable) whilst in the layered compounds, the transition metal valence is most straightforwardly controlled by the oxygen stoichiometry.

4.1 Cation Substitutions in Double Perovskites

Rare-earth elements are usually used in the electron doping of an alkaline-earth metal (and *vice versa*) since their ionic radii are close to each other, thus making the entry of the substituent into the structure easier. From the perspective of the *B* cation ordering, the substitution can either enhance or hinder the degree of order. Trivalent La for divalent Sr substitution on disordered Sr_2FeVO_x[90], Sr_2FeTaO_6[I,II] and Sr_2MnSbO_6[91] enables the formation of, at least partially *B*-site ordered double perovskite through the reductive effect on trivalent Fe, whilst the same doping on the already ordered Sr_2FeMoO_6 lowers the degree of *B* cation ordering as its intrinsic valence mixing[16] is hindered[92-94]. When the total oxygen content is determined, usually by wet-chemical or thermogravimetric analysis, the effects on the valence states are best monitored with different substitution amounts. This allows use of the system as an internal reference complemented with external materials, as observed in many studies[91,95,I,II].

Hole-doping into layered $RBaCo_2O_{5+\delta}$ double perovskites by means of aliovalent A^{II}-for-R^{III} cation substitutions was reported not to affect the Co valence state, instead the charge difference was balanced by the oxygen content.[96] In general, some compensation by oxygen stoichiometry has been observed also in the triple layered $RBa_2Cu_3O_{6+\delta}$ (or $CuBaRCu_2O_{6+\delta}$) perovskites for which hole doping has been employed to introduce superconductivity but the average Cu valence state was also increased by the substitutions[97-99].

4.2 Oxygen Content Control in Double Perovskites

Out of the few non-stoichiometric *B*-site ordered DPs, $Sr_2MgMoO_{6-\delta}$ is maybe the best known material having vacancies of about $\delta = 0.05$ once synthesized under reducing conditions. Vacancies are crucial for its emerging potential as a highly tolerant anode in SOFCs[100]. The highest amount of vacancies is found in the compound with the lowest degree of order, that is, the vacancies are located between crystallographically misplaced Mo atoms whose valence differs from the majority Mo atoms[101]. When the *B* cations are practically fully ordered, the amount of oxygen vacancies is insignificant. Similar results were observed for other *B*-site

ordered double perovskites[102]. An interesting observation was that a poorly-ordered Sr_2FeMoO_6 (g_B = 0.69; S = 0.38) has about same amount of vacancies as $Sr_2MgMoO_{6-\delta}$. It seems possible that, in general, the oxygen nonstoichiometry in the B-site ordered double perovskites is dependent on the degree of order and as most of the time high ordering is the desired target, this point has not been extensively studied. If vacancies are desired, Sr_2FeMoO_6 offers an example of two methods for lowering the degree of order; kinetics and thermodynamics related to the cation ordering[20] or cation substitutions[103]. In these studies, oxygen vacancies were not investigated but can be assumed.

In the A-site ordered $RBaCo_2O_{5+\delta}$ compounds the Co valence state is tuneable by the total oxygen content control. The oxygen content can be adjusted either by TCOD[67,104] or in a glass ampoule with a precise amount of oxygen getter[85,86]. In TCOD, sample is heated to temperatures where oxygen is gradually lost and the desired oxygen partial pressure is adjusted *via* the gas flow. In the ampoule technique, a quantitative reaction of a metal and oxygen is applied. Both methods require knowledge on the start-up stoichiometry. The $RBaFe_2O_{5+\delta}$ compounds behave identically with the B = Co phases so that δ is practically a free integer[78] but $RBaMn_2O_{5+\delta}$ is an exception as only values δ = 0, 0.5 and 1 are obtainable[30,31,66,87].

4.3   Valence State Determination

The valence state determination of the transition metal cations is crucial not only for their role in the material properties but also in the formation of the double perovskites. The techniques for their accurate determination are important to control and the ones used in this work are briefly outlined below.

Wet-Chemical Methods

The transition metals in oxide materials are often at multiple valence states that can be reduced to their lowest oxidation state. The material is dissolved in diluted acid and reduced with an excess amount of reductant. Based on the known reactions and amount of products,

the average valence state of the cation can be calculated. There is a wide range of possible RedOx methods and the titrants are chosen depending on the particular transition metal.

Iodometry is a widely used method and commonly applied for Cu and Co[12,104,105,**III-V**]. It is also applicable for Mn although reports are rare as the solubility of manganese oxides is generally low. The dissolved high-valent ions are reduced with excess KI to their low-valent iodides and the simultaneously formed iodine is reduced with thiosulphate solution in the presence of starch indicator. As the dissolved oxygen in the solvent and its acidity catalyzes the iodide oxidation to iodine, the solvent needs to be deoxygenated under a constant protective gas flow and the titrations carried out quickly without exposure to air. The limitations of the method are mainly related to the solvent; iodometry tolerates only diluted acids, otherwise erroneous results are easily obtained. Cerimetry is more commonly used for iron-containing samples but is also applicable for Co and Mn. In the cerimetric method, a known amount of Fe^{2+} ions are used as reductant for high-valent species and the remaining amount are oxidized with tetravalent cerium sulphate solution using ferroin as an indicator[104,106,**I,II**]. As the sulphate ion readily precipitates alkaline-earth ions, cerimetric titrations are often avoided if these cations are present.

Thermogravimetry

Thermobalance can be used to study the total oxygen content by decomposing the material in a H_2 atmosphere and the original composition can be calculated from the total weight loss, providing the decomposition products are known and stable. Minor limitations exist with some compounds and their decomposition products but on the other hand, if the samples are not easily dissolved or even insoluble, thermogravimetry (TG) provides information on the stoichiometry that would otherwise be difficult to ascertain. In this work, it was observed that compounds containing metals that produce uncertain (PrO_x, EuO_x TbO_x) or hygroscopic (La_2O_3) decomposition products, suffer from inaccurate results when compared to wet-chemical methods. The validity of the latter was established by the material properties[**V**]. Thermobalance is also a practical tool when studying the mass gain or loss in the oxide perovskites. TG analysis gives highly accurate information on the total amount of the labile oxygen and the reversibility of the reaction(s) and stability of the materials is easily verified when combined with XRD measurements.

Mössbauer Spectroscopy

In iron-containing oxides, [57]Fe Mössbauer spectroscopy provides a useful tool to investigate the distribution, valence state and local surroundings of a Fe nucleus in the structure. Particularly, the local environment around Fe is seen as the coordination sphere affects the energy levels of the atom. The Mössbauer active nucleus absorbs and emits a γ quantum (in this case produced by a [57]Co source) without recoil or thermal effects to the lattice[107]. The chemical interactions between the nucleus and environment are detected as small changes in the energy absorbed by the nucleus. As a result, the peak positions move and/or split in the Mössbauer spectrum and the value of the shift is known as an isomer shift (or chemical shift), proportional to the valence state and bonding of the atom. [57]Fe Mössbauer spectroscopy has proven to be valuable method when studying the Fe valence states of double perovskites, especially when they present mixed valence[16,92-94] or charge ordering[33]. In the work outlined here, [57]Fe Mössbauer spectroscopy was used to study the iron valence states in the electron-doped $(Sr,La)_2FeTaO_6$ double perovskites[II].

XANES Spectroscopy

The XANES (*X-ray absorption near-edge structure*) technique utilizes the information obtained from the pre-edge absorption region in the X-ray absorption spectrum. This specific energy region contains information about the excitations that occur when the inner-core electrons transfer to the empty states in outer orbitals. The X-ray absorption energy is proportional to the oxidation state of an atom; therefore a change in the energy indicates a change in the oxidation state.

In the present case, Fe and Ta L-edge XANES was used in qualitative terms to study the valence states of an electron-doped $(Sr,La)_2FeTaO_6$ system[I]. The Fe $L_{2,3}$ -edge spectrum was obtained in the energy range of 700-725 eV when the $2p$ core electron is excited to the empty $3d$ states. The transitions are $2p_{3/2} \rightarrow 3d$ and $2p_{1/2} \rightarrow 3d$ for Fe L_3 and L_2, respectively.[19,95,108,109] The L_3 peaks have higher intensities and therefore they are typically used in the interpretation. The relative intensity ratio of the absorption at 709 and 707 eV corresponds to the ratio of trivalent and divalent Fe[19,95,108,109,I]. Fe_2O_3, Fe_3O_4 and FeO were measured as references for the oxidation states of III, III/II and II, respectively. The Ta L_3 -

edge absorption spectrum is obtained in the energy range of about 9870-9900 eV and Ta_2O_5 was measured as a reference for the Ta^V state[I].

5 CATION ORDERING IN $(Sr_{1-x}La_x)_2FeTaO_{6-\delta}$ SYSTEM

In Sr_2FeTaO_6 compound, the *B*-site cations Fe^{III} and Ta^V tend to place themselves in a disordered manner within the structure due to the small charge and size difference between the *B* cations[27,28,I]. The required difference in charge and size to obtain an ordered compound can be introduced by doping the *A* site with a higher valent cation. If the substitution reduces the oxidation state of Fe^{III} more strongly than that of stable Ta^V, the effect should be enough to enable the formation of an ordered structure. As a result, changes in the magnetic ordering and conductivity could be expected due to the altered electron configuration of the *B* cations.

In the present work, the parent Sr_2FeTaO_6 was substituted with various amounts of trivalent La up to its solubility limit. The entry of the La into the perovskite structure required a more reductive atmosphere than the synthesis of the pristine compound and longer synthesis time with increasing substitution level[I].

5.1 Structural Aspects of the Fe and Ta Ordering

The parent Sr_2FeTaO_6 or $Sr(Fe_{0.5}Ta_{0.5})O_3$ is essentially a simple perovskite with an orthorhombic $\sqrt{2}a_p$ x $\sqrt{2}a_p$ x $2a_p$ unit cell[28]. As the lanthanum substitution starts to effect, the unit cell begins to double in all dimensions as Fe and Ta are located at least partially in an ordered manner. This is evidenced by the appearance of new Bragg reflections originating from the superstructure edges in the diffraction patterns. As the amount of La^{III} is increased, the growing intensity of the supercell peaks becomes evident[I,II] as presented in Figure 3. Two sample series', denoted as A and B, prepared at different temperatures with various doping amounts were studied[I,II].
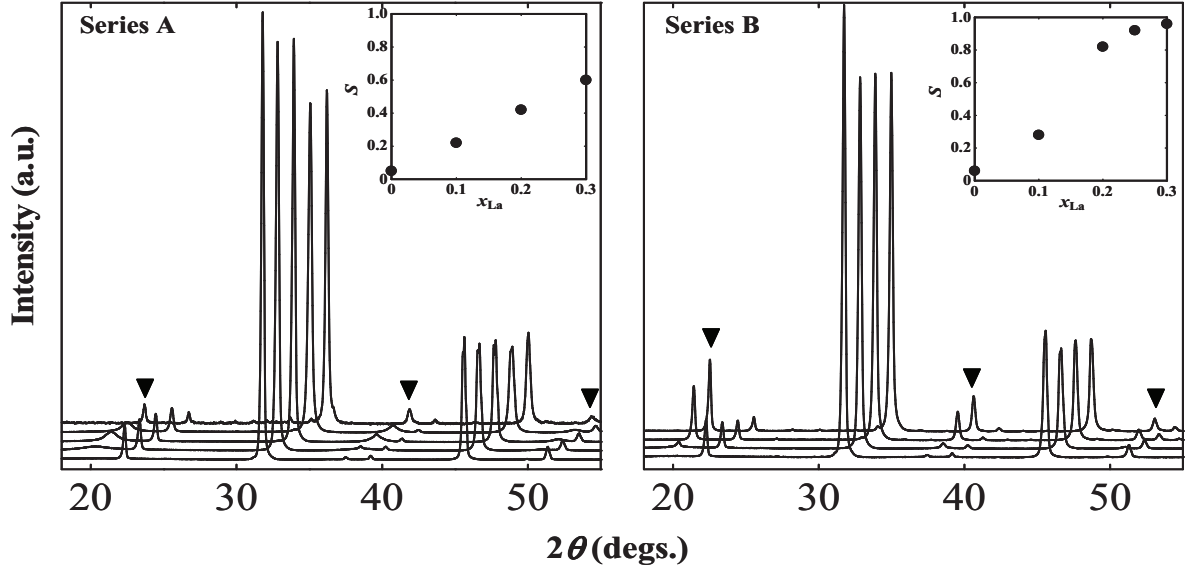
Figure 3. The XRD patterns of $(Sr_{1-x}La_x)_2FeTaO_{6-\delta}$ for Series A (x = 0.0, 0.1, 0.15, 0.20, 0.30) and Series B (x = 0.0, 0.1, 0.20, 0.25, 0.30). Arrows indicate the Bragg reflections from the supercell edges. The insets show the degree of order (S) for each compound.

Indexing of the diffraction profiles confirmed that the tetragonal $I4/m$ symmetry, common for B-site ordered DPs with A = Sr could be excluded with certainty based on the appearance of additional Bragg reflections this space group does not explain. Instead, the octahedral tilting often leads to a monoclinic symmetry with $P2_1/n$ space group (through $a^-b^+c^-$ tilting in Glazer's notation[110]) in the B-site ordered DP structure[42,I]. The structural model was constructed based on the suggestion of the Structure Prediction Diagnostic Software (SPuDS)[48] that also indicated the aforementioned space group as the most reasonable option. The refined fractional occupancies of Fe and Ta and thereby calculated degree of order, S, confirmed an increasing trend in the B cation long-range order with increasing substitution. The maximum degree of order obtained for the highest-doped sample of x = 0.30 (containing a small amount of impurity) was S = 0.60(1) and 0.96(1) for Series A and B, respectively[I,II]. The domain-type of ordering suggested for the Series A based on broad supercell reflections[50,I] is not observed for the Series B samples prepared at the higher temperature; the full-width half maxima (FWHM) of the doubled cell are identical to the fundamental Bragg reflections[II].

As the degree of order could be increased by the higher synthesis temperature, the system points to a kinetically controlled ordering as found for other DP oxides[50,77]. Impurities

20

appeared if the synthesis time was increased in attempts to increase the degree of order (and solubility limit of the substituent).

The lattice behavior was investigated for both Series A and Series B. The increase of the substitution expands the lattice parameters and cell volume even though La^{III} is smaller than divalent Sr[74] The explanation for the cell enlargement is that while the La^{III} reduces the valence of B cations, their ionic radii become larger, overcoming the substituent size effect. Similar behavior is seen *e.g.* in the substituted $(Sr_{1-x}La_x)_2FeMoO_6$ system[92]. For the Series A, the lattice parameters are somewhat scattered but the cell volume is increasing[I]. In the Series B with higher degree of order, all the lattice parameters showed an increasing trend throughout the substitutions[II].

5.2   Effect on Valence States and Magnetic Properties

The valence states of the B cations were monitored by XANES spectroscopy, Mössbauer spectroscopy and chemical analyses. Based on the Fe $L_{2,3}$ edge spectrum, the Fe^{III}/Fe^{II} ratio decreases gradually with increasing electron doping. The shift in the absorption maximum in Ta L_3 spectrum could indicate a minor decrease in the average valence for Ta^V also[I]. For both Series A and B, the ^{57}Fe Mössbauer spectra indicated the presence of three different Fe components in the substituted samples which were indentified as divalent and trivalent Fe, the latter being in two different surroundings[II]. The magnetic properties show an antiferromagnetic-type transition at 15-25 K in both parent and ordered samples with a slight increase of transition temperature along with the degree of order[I,II]. The parent phase has been determined as a spin-glass by a previous work[28] but the methods used here do not allow this interpretation. The Weiss constant θ_p (calculated from the Curie-Weiss fit) is negative for the samples with the substitution level $x = 0$ and 0.1, in agreement with the antiferromagnetic behaviour but turns positive with $x = 0.2$ and above in both Series A and B. The slightly positive Weiss temperature (~18 K at its highest) could indicate minor ferro/ferrimagnetic interactions in these compounds. More recently, similar research was reported for $(Sr_{1-x}La_x)_2MnSbO_6$ ($x = 0.5$) where short-range ferromagnetism above $T > 90$ K was successfully evidenced although long-range antiferromagnetic ordering was clear at low temperature[91].

6 CATION AND OXYGEN ORDERING IN LaBaCo$_2$O$_{5+\delta}$

The interplay between disordered and ordered phases of the same compound became of large interest after a significant increase in Curie temperature was discovered for the ordered CMR LaBaMn$_2$O$_6$ compound compared to its disordered polymorph[30]. Later, disordered and ordered forms were described also for the PrBaMn$_2$O$_6$[111]. In the family of RBaCo$_2$O$_{5+\delta}$, only R = La compound has so far shown the ability to exist in both disordered[112] and ordered[63] manner, depending on the synthesis conditions. In this work, compounds with $\delta = 1$ in all the existing phases were revisited and a new nano-scale ordered compound was evidenced and characterized[III]. The synthesis of the new, A-site and oxygen vacancy ordered compound with $\delta = 0.5$ stoichiometry was established and characterized by structural and physical property features[IV]. Figure 4 illuminates the synthetic pathways and the role of the $p(O_2)$ in the formation of each studied LaBaCo$_2$O$_{5+\delta}$ compounds:
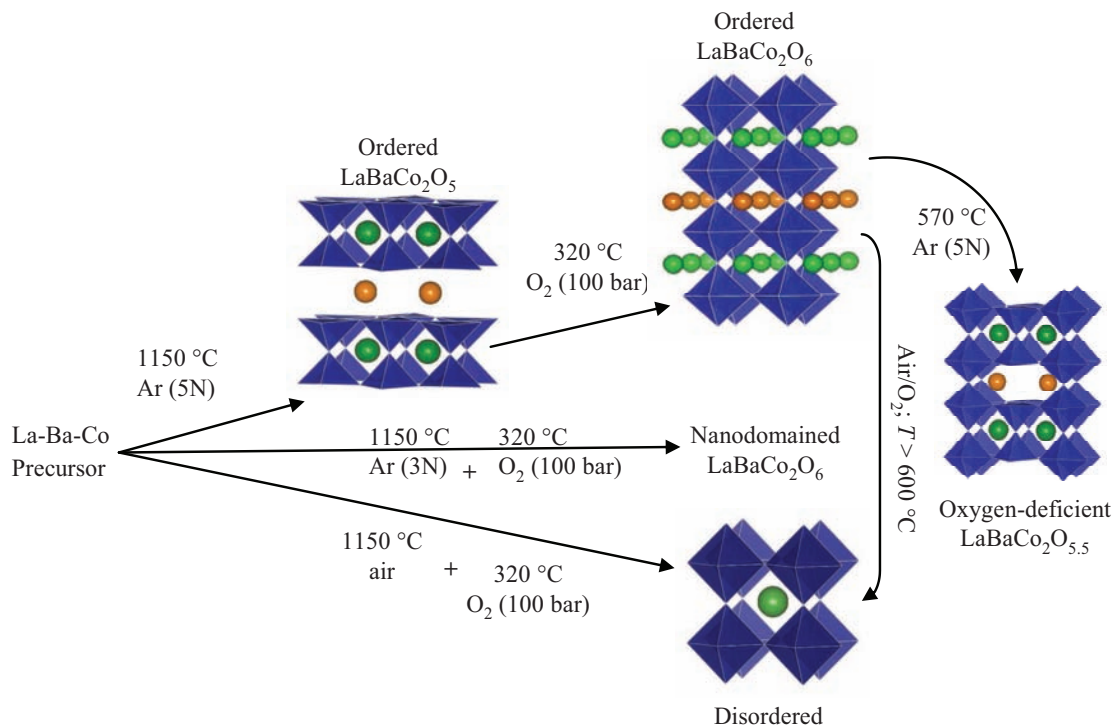

Figure 4. The role of $p(O_2)$ and synthesis conditions for the differently ordered LaBaCo$_2$O$_{5+\delta}$[III,IV].

6.1   A site Disorder *versus* Order in LaBaCo$_2$O$_6$

Disordered La$_{0.5}$Ba$_{0.5}$CoO$_3$ crystallizes as cubic perovskite, the large *A* constituents stabilizing the high symmetry[63,112]. When synthesized under low p(O$_2$), an ordered structure with altering LaO$_\delta$ and BaO layers is obtained[63,I] and can be oxygenated to full stoichiometry in where all the vacancies are filled and the Co^{III} and Co^{IV} cations adopt an octahedral coordination. The structure is described as an *A*-site ordered DP with a_p x a_p x $2a_p$ doubling in a tetragonal *P*4/*mmm* unit cell[63,I]. In this work, a third polymorph was discovered that is a combination of the disordered and ordered forms[III].

The details were established in a HRTEM study that revealed the compound consisting of a few nanometer-sized structural domains. These blocks are oriented in 90° angle to each other in all three directions and the structure inside the domains is of ordered LaBaCo$_2$O$_6$. The domains cause anisotropic strain broadening along <100>$_p$ in the XRD patterns in an otherwise cubic-like diffractogram. Figure 5 presents the observed selected-area electron diffraction (SAED) patterns and a scheme of the structure formation.
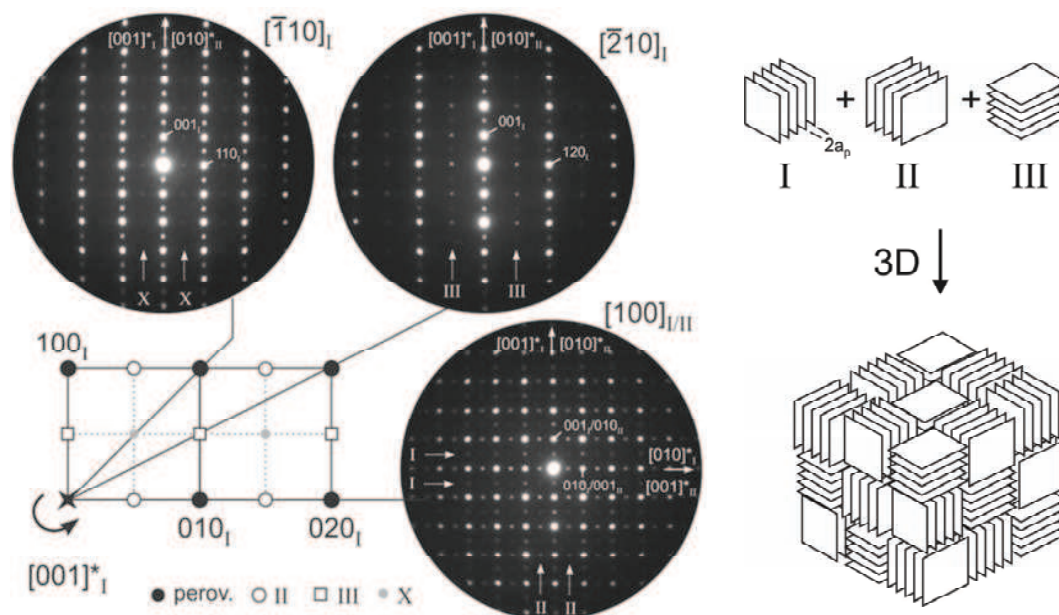
Figure 5. Typical SAED patterns observed for the nanoscale-ordered LaBaCo$_2$O$_6$. The <100>p zone axis patterns (ZAP) displayed in (a) are the most characteristic. In (b), the rows of weak reflections indicated by arrows are not compatible with the two 112-type domains observed in (a). In (c), the rows of very weak reflections indicated by arrows are associated to a secondary phase denoted as X. For more a detailed description, see Fig. 4. in publication **III.** *Reprinted by the permission of ACS.*

The physical properties of the nanostructured compound differ from the previously known polymorphs but resemble more those of the cubic structure[113,III]. The most significant difference was observed in the magnetic properties; although all the polymorphs are ferromagnetic with practically identical Curie temperature ($T_C \approx 175$ K)[III], the nanodomained compound has highly anisotropic ZFC and FC magnetic susceptibility. In addition, the material is a hard ferromagnet with coercive field of $H_c \approx 0.4$ T while the other compounds as soft ferromagnets have much smaller coercivity. These findings were explained by a spin-locking effect induced by the nanodomained structure[113]. It is worth noting that the nanodomained structure was observed in various oxygen stoichiometries under the same synthesis conditions but was oxygenated to the full extent for comparative reasons.

6.2 The Oxygen Deficient LaBaCo₂O₅₊δ (δ = 0.5)

LaBaCo$_2$O$_{5+\delta}$ ($\delta = 0.5$) is the newest member in the series of layered, oxygen vacancy ordered compounds that have intrigued researchers for over a decade due to their peculiar crystal structure, magnetic and transport properties and magnetic structure. The synthesis technique was adopted from the conditions used for LaBaCo$_2$O$_6$[63,III] and LaBaMn$_2$O$_{6-\delta}$[30]. In total, a three-step synthesis is required in where the readily-obtained material is first oxidized to full stoichiometry and then oxygen depleted to the target stoichiometry at 570 °C for 12 h in constant Ar (5N) flow. Finally, to ensure proper oxygen vacancy ordering, slow furnace cooling to room temperature (RT) was applied. Wet-chemical analysis indicated the presence of a slight excess oxygen giving LaBaCo$_2$O$_{5.52}$ as the final composition[IV].

The NPD patterns were recorded at various temperatures between 10-410 K. Patterns reveal the presence of magnetic contributions already in the RT pattern, the observation being consistent with the measured magnetic properties. Therefore the magnetic model needed to be taken account already in the combined XRD and NPD refinement of the RT data for gaining accurate wavelength and peak shape parameters. Indexing led to an orthorhombic symmetry and based on the refinements, LaBaCo$_2$O$_{5+\delta}$ ($\delta = 0.5$) compound has an orthorhombic *Pmmm* structure applied to a_p x $2a_p$ x $2a_p$ unit cell, common to all RBaCo$_2$O$_{5+\delta}$ ($\delta = 0.5$) phases[12]. Oxygen vacancies are located in the LaO$_\delta$ layer and order with oxygen sites so that the Co^{III}

ions alternate in octahedral and pyramidal coordination (see Figure 4). The small amount of excess oxygen evidenced was successfully modeled into the LaO_δ layer and the final oxygen content was $\delta = 0.54(1)$, which correlated with the wet-chemical analysis. Refinement of the occupancy factor of the two oxygen sites in this layer also revealed that a portion of the oxygen ions are misplaced from their correct crystallographic sites. Combining this information with the ED and HRTEM observations, it was possible to identify that the compound contains a fraction of another superstructure indexed as *Cmmm* with $2a_p$ x $4a_p$ x a_p multiplication, similar to that found for the $LaBaMn_2O_{5+\delta}$ ($\delta = 0.5$) compound[IV]. In addition, the refinement of the fractional occupancies of the *A* cations La and Ba indicated an incomplete La/Ba long-range order ($g_{La/Ba} = 0.888(2)$; $S = 0.776(2)$). The degree of the *A*-cation disorder in this case is close to the level of oxygen vacancy disorder and the Rietveld refinement did not indicate a significant correlation ($< 50\ \%$) between the *g* of La/Ba and the two O sites in the LaO_δ layer.

The magnetic properties resemble those of the other oxygen vacancy ordered, layered cobaltates, that is the compound undergoes a spontaneous magnetization effect from paramagnetic to ferrimagnetic (saturation magnetization only ~0.16 μ_B/Co at 5 T) at $T_C = 326$ K and then turns abruptly into an antiferromagnetically ordered structure[12]. The Rietveld refinements of the magnetic structure indicate a *G*-type ferrimagnetic ordering (coupling of moments along *ab* plane) in the temperature range of 245-290 K which then turns into *G*-type antiferromagnetic ordering below 245 K. There is no detectable change in the magnetic reflections except their increasing intensity towards the lower temperature. The refined magnetic moments indicate an intermediate spin state for Co[III] from 10 to 290 K. This makes the compound different from similar compounds with smaller R^{III} cation for which secondary antiferromagnetic phases, accompanied by possible spin-state transition, have been detected[114,115]. The effective paramagnetic moment, calculated from the Curie-Weiss fit of the magnetization data between 330-400 K gives a value of 3.72 μ_B/Co[IV].

The expected spin-only value can be calculated as

$$\mu_{SO} = Lg\sqrt{S(S+1)}, \tag{2}$$

where S is the spin quantum number and $g \approx 2$ if the orbital angular moment L is estimated insignificant[116].

The possible electronic configurations of a Co^{III} are low spin (LS, t_{2g}^6; $S = 0$), IS ($t_{2g}^5 e_g^1$; $S = 1$) and HS ($t_{2g}^4 e_g^2$; $S = 2$) and their mixtures, for which the moments are calculated as follows[116]:

$$\mu_{A:B} = \sqrt{\frac{1}{2}\mu_{SO}(A) + \frac{1}{2}\mu_{SO}(B)}. \tag{3}$$

This gives $2.83\mu_B$ and $4.90\mu_B$ for the pure IS and HS, respectively and $2.00\mu_B$ and $4.00\mu_B$ for the 1:1 mixtures of LS/IS and IS/HS, respectively (calculated *per* Co). This would indicate that above T_C, Co^{III} is at least partially a mixture of two spin states as the experimental value is more closer to LS/HS Co^{III} mixture than pure IS Co^{III}.

7 CHEMICAL PRESSURE EFFECT

Chemical pressure effect is understood as the changes arising in compounds when a cation is substituted for another without changing either the charge balance or the element responsible for the physical properties of the compound. This type of substitution provokes the system through the size difference between the replaced cations without dramatically manipulating the material properties. This is best facilitated by replacing an earth-alkaline or a rare-earth cation for another. The structural effect can involve even a change of the symmetry of the compound as often observed with earth-alkaline substitutions,[25,92,117] or the changes can be more modest as most of the time observed in the R cation substitutions[12]. In this thesis, the chemical pressure effect was studied by means of electronic band structure calculations for the halfmetallic B-site ordered DPs and experimentally by crystal-chemical features and physical properties for the layered $RBaCo_2O_{5+\delta}$ ($\delta = 0.5$) compounds[V].

7.1 Electronic Structure of A_2FeMoO$_6$ (A = Ca, Sr, Ba)

In the A_2FeMoO$_6$ double perovskites, the alkaline-earth cation is easily exchangeable to another kind. Replacing A = Ba by smaller Sr and Ca lowers the symmetry from cubic to tetragonal and monoclinic, respectively. The exchange affects the Curie temperature in such a way that A = Sr has the highest T_C of about 420 K[10] while A = Ba and Ca fall closer to room temperature[14,26]. All the compounds have shown experimentally a large TMR effect and they have been determined to be halfmetals by band structure calculations[10,14,21,26].

The electronic band structure of a compound is the key for understanding many of its material properties. The band structure is a link between the crystal structure, bonding and electronic as well as optical properties. For a continuous structure, the band structure is in fact a molecular orbital diagram where the translational symmetry of the crystal is taken into account[118]. The density of states (DOS) of the occupied states is gained by integrating the band structure diagram between certain energy levels.

The methods for calculating an electronic band structure are based on the density functional theory (DFT)[119] combined with local-density approximation (LDA)[120] method. The calculations may experience problems if the studied compound possesses strongly correlated electrons, as is the case with double perovskites, and therefore several improvements on the calculation methods have been introduced. Perhaps the most common method is to add a correction potential U in the approximation, a so called on-site Coulomb correlation correction[121,122]. As a very simplified explanation, instead of using an average Coulomb energy for the d-d (or f-f) electron interaction, the calculation is performed with more accurate terms. A commonly accepted type of calculation is an exchange correlation potential of von Barth-Hedin[123]. As a rule of thumb, it can be said that LDA is used when the compound has delocalized s and p electrons whereas LDA + U is favored if the compound has localized d (or f) electrons. However, if a reasonable solution is achieved without using any correction terms, the result can be considered acceptable[124]. Usually the need for adding correction terms arises if the gaps in the density of states are smaller than those experimentally found or lacking completely, and/or the values of spin and orbital moments are too low[121]. The band structures here were calculated using the program ABCAP v1.0 (All-electron Band-structure CAlculation Package)[125] adopting the full-potential linearized augmented plane wave

(FLAPW) method[126] based on the LDA and 216 special k points in the irreducible Brillouin zone were used. A perfect order of the B cations was assumed and the valence states were treated as Fe^{III} and Mo^V. The reliability of the cycles was monitored by the number of electrons inside the "muffin tin" radius and the by the obtained total magnetic moment (close to 4 μ_B).

The purpose of the calculations in the present work was to see how well the obtained band structures correlate with the experimental data. All the calculations were performed with the correct crystallographic structure adopted from references. In some of the calculations, both LDA and LDA + U (U = 1.0 eV[127]) were applied but as no significant difference was observed, the calculations were completed with the LDA method. Figure 6 shows the calculated band structure of the Sr_2FeMoO_6 and the zoomed densities of Fe $3d$ and Mo $4d$ states for $(Ca,Sr,Ba)_2FeMoO_6$ compounds, calculated using the reported NPD structural data[25,117] are shown as a basis for the discussion.

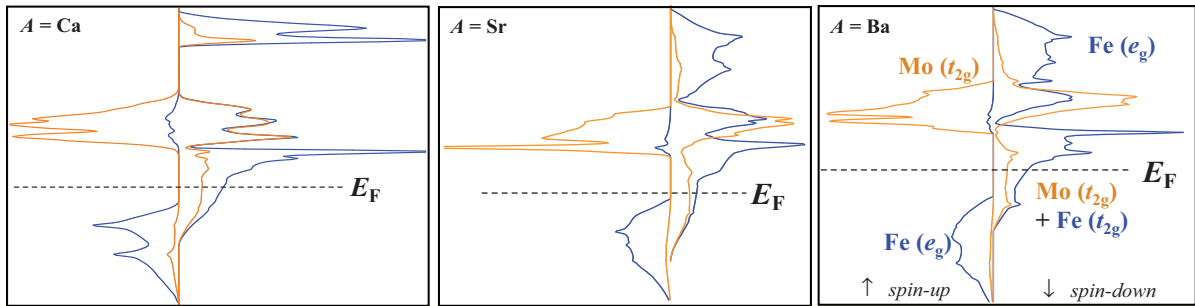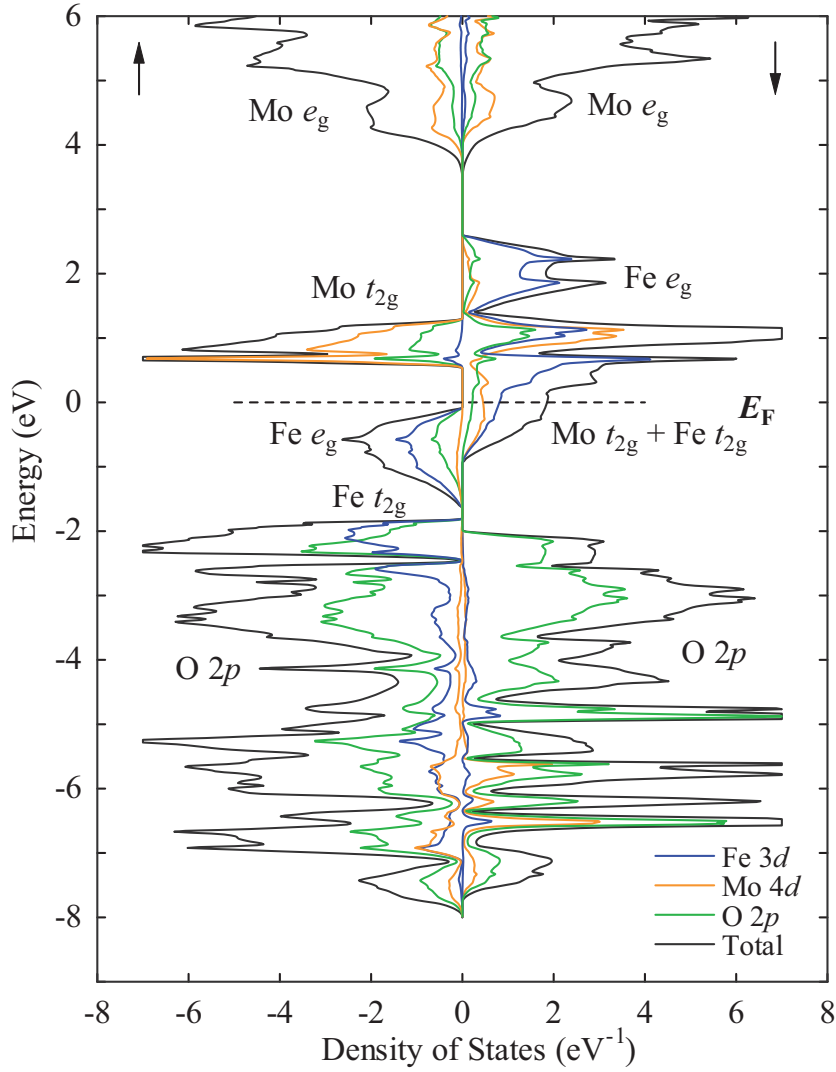**Figure 6.** (top) The electronic band structure of Sr_2FeMoO_6 and (bottom) the Fe and Mo density of states for $(Ca,Sr,Ba)_2FeMoO_6$ in the vicinity of the Fermi level. The Fe t_{2g} (↑) fall below and the Mo e_g states above the zoomed areas.

On the up-spin side is a gap in the density of states while the conducting states on the down-spin side cross the Fermi level in accordance with the spin-polarized band structure (halfmetallicity), caused by the hybridization of both Mo and Fe t_{2g} states[10,127]. The splitting

of the hybridized Mo and Fe DOS of A = Ca compound is caused by the lower symmetry compared to that of A = Sr and Ba compounds[21]. The area (calculated by numerical intergration) of the Mo $4d$ DOS below the E_F show that the area decreases when the size of A cation increases. The difference between Ca_2FeMoO_6 and Sr_2FeMoO_6 compounds is small but a clear difference can be observed when compared to Ba_2FeMoO_6. The area of occupied states is proportional to their spin density and therefore a decrease in the area of Mo $4d$; t_{2g} indicates a lessened electron density in those states. In practice, the result means that in the Ba_2FeMoO_6 compound the itinerant electron of Mo^V is likely to transfer a bigger part of its charge and spin density to Fe^{III} than with A = Ca and Sr compounds and this is seen as a decrease in the occupied Mo spin band below the E_F. When a bigger portion of the charge and spin density is on the Fe site, the valence of Fe decreases close to II and, in proportion, the valence of Mo increases close to VI. This result is in good agreement with the experimental results of ^{57}Fe Mössbauer and XANES spectroscopy combined with wet-chemical analysis[18]; there is only a small difference in the Fe valence between A = Ca and Sr compounds but A = Ba differs from the previous ones by having Fe valence close to II. The experimental data[18] and the calculated Mo $4d$ DOS below E_F are combined in Figure 7.
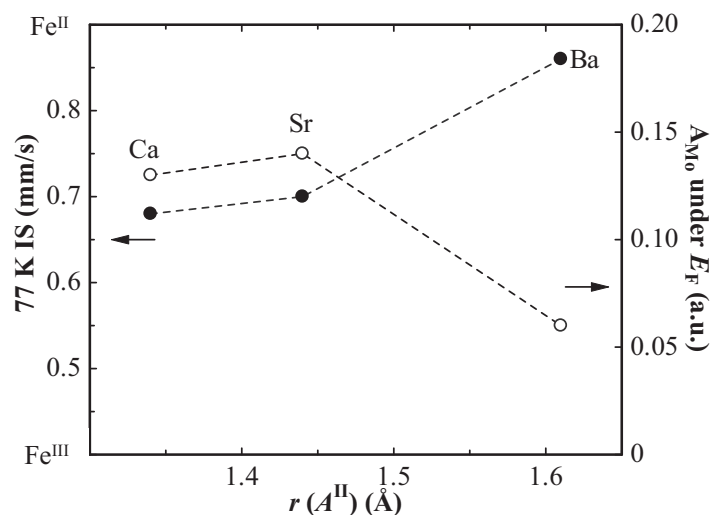

Figure 7. The experimental Fe valence drawn as isomer shift values from Mössbauer analysis[18] (filled dots) and the area of Mo DOS below E_F (hollow circles), inversely proportional to the Fe valence state. The Fe valence states judged by the isomer shift values[107] are marked to the axis on the left.

7.2   Isovalent Substitution in RBaCo$_2$O$_{5+\delta}$ ($\delta = 0.5$)

The RBaCo$_2$O$_{5+\delta}$ ($\delta = 0.5$) compounds have been studied for a decade due to their peculiar oxygen-vacancy ordered structure and the atypical magnetic properties. Especially the magnetic structure at the low temperature has gained the interest of many researchers. All the compounds have been found to undergo a spontaneous magnetization which then turns into antiferromagnetic (AFM) ordering on further cooling. Most typically, the existence or lack of a secondary AFM ordering at the low temperature region has raised questions. Usually the magnetic properties are in line with the NPD data, that is, the presence of a secondary magnetic structure is supported by the magnetization behaviour. The magnetic and transport properties of these compounds are highly sensitive for the actual Co valence, directly dictated by the total oxygen content of the compounds. Difficulties have appeared as the $\delta = 0.5$ stoichiometry is not readily obtained but the compounds tend to form at least slightly under- or over-stoichiometric which affects the material properties. In addition, there are other stable superstructures with different δ value besides the best known $\delta = 0.5$ composition whose properties have also been subject to research interest (discussed in Chapter 3).

In this thesis, the chemical pressure and Co valence effects were studied in RBaCo$_2$O$_{5+\delta}$ ($\delta = 0.5$) phases (R = Y, Ho-Sm, Nd, Pr and La) with precisely adjusted oxygen content. The idea was to establish the sensitivity to the correct stoichiometry in these compounds. The effects of $r(R^{III})$ and δ parameter were studied by means of lattice behavior, magnetization and calorimetric effect of the metal-insulator transition (T_{M-I}) appearing above room temperature. Figure 8 illustrates the R^{III} size and oxygen content effect on the unit cell.
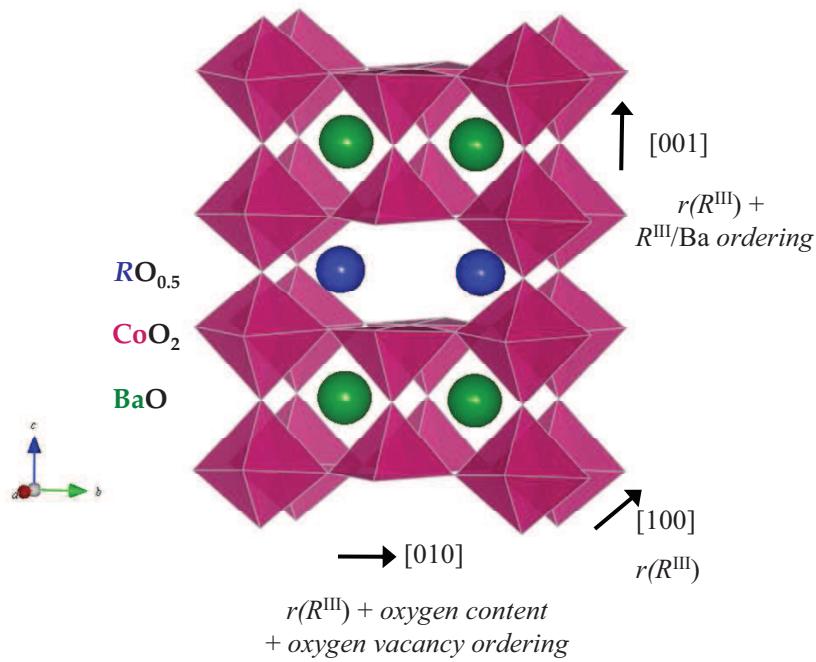
Figure 8. Factors affecting the a_p x $2a_p$ x $2a_p$ superstructure (*Pmmm*) of RBaCo$_2$O$_{5+\delta}$ (δ = 0.5). *Reprinted by the permission of Elsevier B.V.*

The results were compared with the literature results on the same compounds that have been addressed to represent the $\delta = 0.5$ phases. Comparison of the lattice parameters of the adjusted samples and the literature data show a linear increase in the *a* parameter along increasing $r(R^{III})$, *i.e.* the parameter is not affected by the small deviations in the oxygen content whereas a strong sensitivity is observed along the *b* axis as indicated by the scattered values of the literature data. Analyses of some off-stoichiometric samples revealed that an increase in the oxygen content causes their *b* axis to decrease and *c* axis to increase. A rather linear increase of the *c* parameter with increasing $r(R^{III})$ is seen for the samples with small and medium-sized rare earth constituents whereas those with R = (Sm), Nd, Pr and La somewhat deviate from the linear behavior. This is attributed to a gradually lowered degree of order within the *A*-cation sublattice. The change in the slope of parameter *b* (about R = Eu) is tentatively attributed to increasing oxygen/vacancy disorder with increasing $r(R^{III})$. Interestingly, the same behavior was observed for the *c* parameter already in the as-prepared samples, *i.e.* the disorder is not induced by the heat treatments performed in oxygen content adjustments.[V] The cell evolution of the *b* and *c* axis is shown in Figure 9.
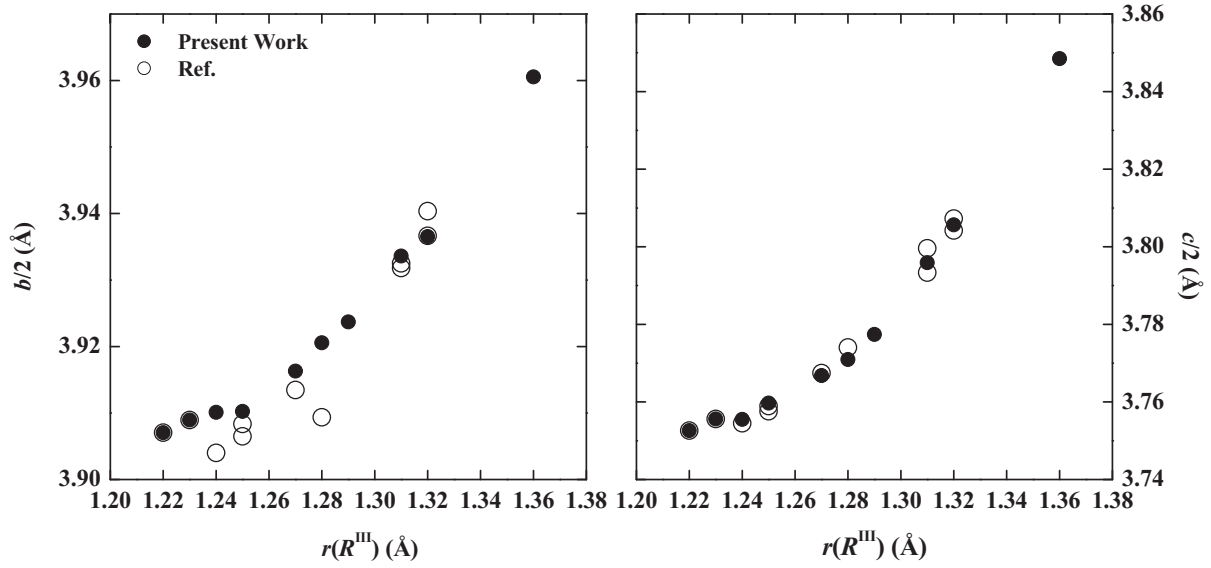
Figure 9. R^{III} size effect on the lattice parameters b and c in the present work (filled circles) compared with reference values (hollow circles)[81,83,84,86,128-132] for $RBaCo_2O_{5+\delta}$ ($\delta = 0.5$) compounds. The effect on a parameter was linear for both datasets. *Reprinted by the permission of Elsevier B.V.*

The effect is so pronounced that a possible change in the Co^{III} spin-state in the compounds discussed for the larger Rs[133] is likely not the only explanation. It is also worth noting that all the compounds, except R = La, are paramagnetic at RT and the T_{M-I} has occurred only for R = Y and Ho compounds[32,V], justifying the comparative discussion. Recent reports have underlined the tendency of the $PrBaCo_2O_{5.5}$ and $LaBaCo_2O_{5.5}$ compounds to exhibit partial oxygen vacancy disorder[81,85,IV] but the ordering of the R and Ba cations has not been really studied. Here, the refinements of the fractional occupancies from XRD data were performed for representative Rs. The results indeed revealed - within the limits of XRD - a certain level of disorder for the R = Sm, Nd and Pr samples with S = 0.98(1), 0.89(1) and 0.82(1), respectively[V] and the NPD data for R = La sample gave S = 0.78(1).

The ZFC and FC magnetization of the oxygen-adjusted, R varied samples showed no traces of secondary magnetic transitions at the AFM region either in the temperature-dependent reciprocal susceptibility $\chi^{-1}(T)$ or in the derivative curves. It was, however, observed that the off-stoichiometric samples undergo secondary transitions in the range of 80-180 K, depending on the R and δ^{V}. Figure 10 demonstrates the stoichiometry effect on the magnetic properties in the $EuBaCo_2O_{5+\delta}$ and $TbBaCo_2O_{5+\delta}$ systems.
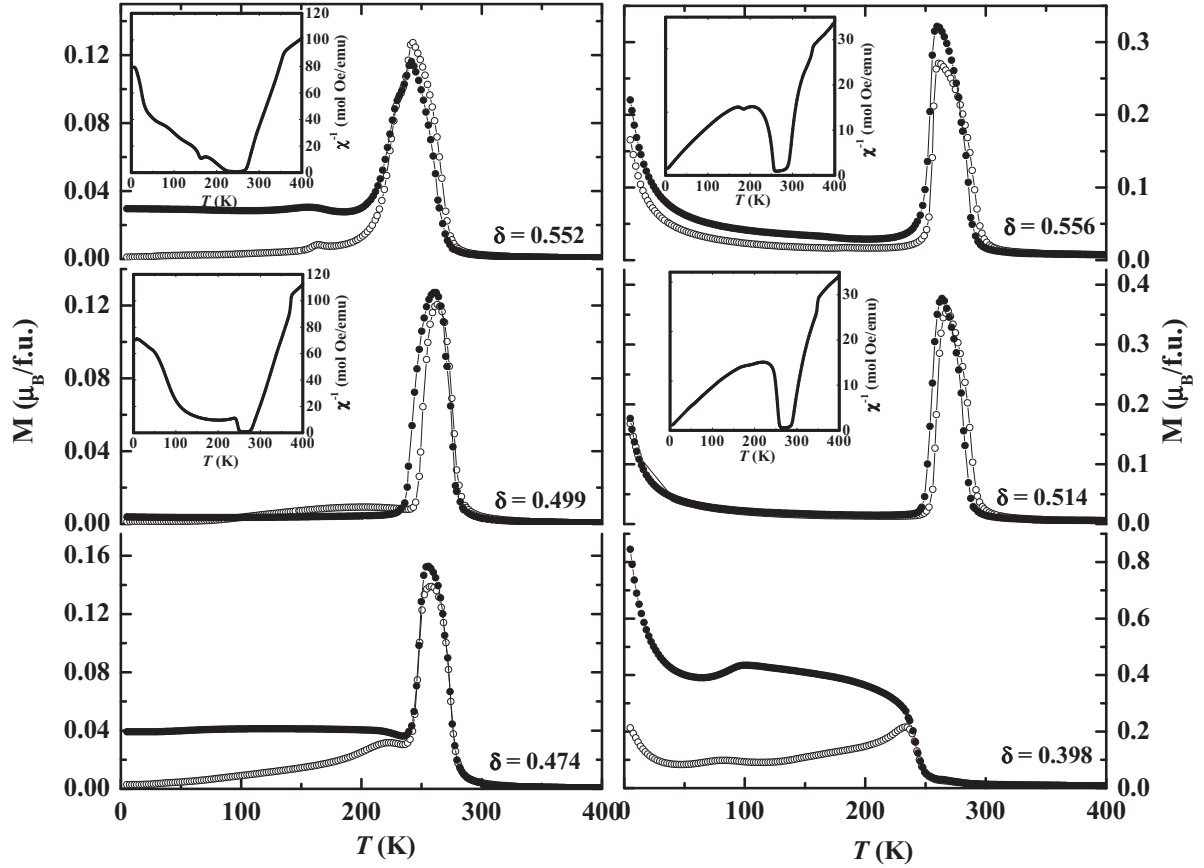
Figure 10. Temperature-dependent ZFC (hollow circles) and FC (filled circles) magnetization of EuBaCo$_2$O$_{5+\delta}$ and TbBaCo$_2$O$_{5+\delta}$ compounds measured for various oxygen stoichiometries (*reprinted by the permission of Elsevier B.V.*) The insets show the reciprocal magnetic susceptibility $\chi^{-1}(T)$.

The ZFC and FC magnetization of the oxygen-adjusted RBaCo$_2$O$_{5+\delta}$ samples merge after the AFM transition but reveal again separation from R = Sm. For the larger Rs, the treatment methods used in this work did not allow high-quality samples in terms of ordering and therefore the observed magnetization is highly anisotropic for R = (Sm) Nd and Pr[V]. The lattice behavior supports these observations as the deviation from the linear trend begins around R = Sm but the results also support the assumption that at some point the series undergoes a spin-state transition that is dependent on the R^{III} size[133]: the effective paramagnetic moments for the end members YBaCo$_2$O$_{5.495}$ and LaBaCo$_2$O$_{5.52}$ are μ_{eff} = 2.49 μ_B/Co and μ_{eff} = 3.73 μ_B/Co, respectively (calculated from the Curie-Weiss fits between 330-400 K). Both these values are for the state after the metal-insulator transition[32,IV,V] but nevertheless, comparable with each other. The Curie temperature is found to decrease with increasing $r(R^{III})$ until R = Pr but the highest T_C is measured for the R = La compound[IV].

The metal-insulator transition involves an enthalpy change[32,86] and can be probed by differential scanning calorimetry (DSC). The results also emphasize the importance of the oxygen stoichiometry for this transition. Figure 11 illustrates the enthalpy difference in the adjusted $\delta = 0.50$ samples with different Rs and several δ values for $EuBaCo_2O_{5+\delta}$.
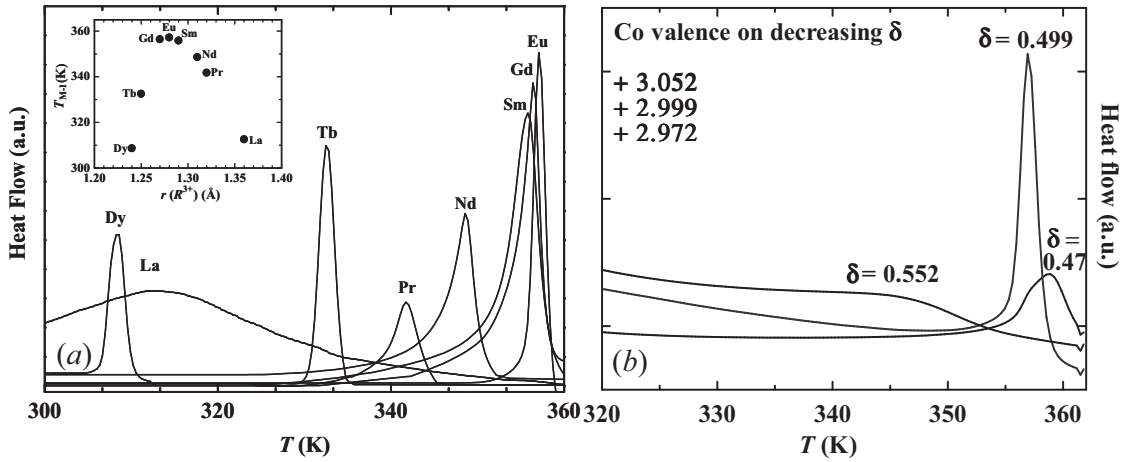
Figure 11. DSC heating curves (20 °C/min) of $RBaCo_2O_{5+\delta}$ for (a) various Rs with $\delta = 0.50$ (*reprinted by the permission of Elsevier B.V.*) and (b) $EuBaCo_2O_{5+\delta}$.

A decrease of enthalpy was found with increasing $r(R^{III})$. This was interpreted to originate from the A-cation and/or oxygen vacancy disorder; given that the samples with the largest Rs contain only 80~90 % of the correct phase, a weakened calorimetric effect seems reasonable[V]. Moreover, the highest calorimetric effect is found for the precisely oxygen-adjusted samples while the enthalpy decreases dramatically compared to slightly oxygen off-stoichiometric members[V].

8 CONCLUSIONS

Understanding the complex relationships between cation ordering, oxygen stoichiometry and metal valence states are essential for the design of new perovskite-related materials and in fine-tuning their properties. In this thesis, the syntheses of two new double perovskite oxides by controlling the above mentioned factors are described and characterized by their structural, chemical and physical properties.

In the $(Sr,La)_2FeTaO_6$ system, the impact of the electron doping through aliovalent La^{III}-for-Sr^{II} substitution on the disordered parent system was studied and a B-site ordered double perovskite with linearly increasing degree of order with increasing substitution was evidenced. The Mössbauer and XANES spectroscopy results verified the gradual decrease of the Fe valence state as a result of the substitution. The wet-chemical analyses indicated essentially oxygen stoichiometric compounds, meaning the charge difference of the A-site constituents is balanced by the electron doping.

The synthesis of the oxygen vacancy ordered $LaBaCo_2O_{5+\delta}$ ($\delta = 0.5$) was demonstrated for the first time. The material was characterized by its structural and physical properties. The crystal structure analysis by NPD combined with ED observations indicated a partial oxygen vacancy disorder so that the compound contains a portion of a secondary superstructure. Results also strongly indicated some degree of disorder in the La/Ba ordering. The possibility of disorder of R and Ba was investigated in the whole $RBaCo_2O_{5.5}$ series (R = Y, Ho-Sm, Nd, Pr). These results support the assumption that the compounds with R = (Sm), Nd, Pr and La are possibly not entirely A-site or oxygen vacancy ordered unless treated under controlled conditions. It was also shown that the total oxygen content control plays an important role in the physical properties of these cobalt oxides.

The band structure calculations of the B-site ordered A_2FeMoO_6 (A = Ca, Sr, Ba) double perovskites were in line with the reported spin-polarized Fermi surface (halfmetallicity) for these compounds. The detailed results were analyzed closely with the experimental findings and their correlation was found to be excellent. It was also noticed that the structural parameters have an effect on the resulting band structures but small discrepancies do not prevent the correct solutions.

REFERENCES

1. F. Galasso, L. Katz, R. Ward, *J. Am. Chem. Soc*. **81** (1959) 820.

2. A.W. Sleight, R. Ward, *J. Am. Chem. Soc*. **83** (1961) 1088.

3. A.W. Sleight, J. Longo, R. Ward, *Inorg. Chem*. **1** (1962) 245.

4. L. Er-Rakho, C. Michel, Ph. Lacorre, B. Raveau, *J. Solid State Chem*. **73** (1988) 531.

5. L. Barbey, N. Nguyen, V. Caignaert, M. Hervieu, B. Raveau, *Mater. Res. Bull*. **27** (1992) 295.

6. W. Zhou, C.T. Lin, W.Y. Liang, *Adv. Mater*. **5** (1993) 735.

7. J.P. Chapman, J.P. Attfield, M. Molgg, C.M. Friend, T.P. Beales, *Angew. Chem. Int. Edit*. **35** (1996) 2482.

8. P. Karen, P.M. Woodward, *J. Mater. Chem*. **9** (1999) 789.

9. C. Martin, A. Maignan, D. Pelloquin, N. Nguyen, B. Raveau, *Appl. Phys. Lett*. **71** (1997) 1421.

10. K.-I. Kobayashi, T. Kimura, H. Sawada, K. Terakura, Y. Tokura, *Nature* **395** (1998) 677.

11. V. Caignaert, A. Maignan, B. Raveau, *Solid State Comm*. **95** (1995) 357.

12. A. Maignan, C. Martin, D. Pelloquin, N. Nguyen, B. Raveau, *J. Solid State Chem*. **142** (1999) 247.

13. K.-I. Kobayashi, Y. Tomioka, H. Sawada, K. Terakura, Y. Tokura, *Phys. Rev. B* **59** (1999) 11159.

14. W. Prellier, V. Smolyaninova, A. Biswas, C. Galley, R.L. Greene, K. Ramesha, J. Gopalakrishnan, *J. Phys.: Condens. Matter* **12** (2000) 965.

15. F. Galasso, F.C. Douglas, R.J. Kasper, *J. Chem. Phys*. **44** (1966) 1672.

16. J. Lindén, T. Yamamoto, M. Karppinen, H. Yamauchi, *Appl. Phys. Lett*. **76** (2000) 2925.

17. J.M. Greneche, M., Venkatesan, R. Suryanarayanan, J.M.D Coey, *Phys. Rev. B* **63** (2001) 174403.

18. Y. Yasukawa, J. Lindén, T.S. Chan, R.S. Liu, H. Yamauchi, M. Karppinen, *J. Solid State Chem*. **177** (2004) 2655.

19. T.S. Chan, R.S. Liu, G.Y. Guo, S.F. Hu, J.G. Lin, J.M. Chen, J.P. Attfield, *Chem. Mater*. **15** (2003) 425.

20. Y.H. Huang, M. Karppinen, H. Yamauchi, J.B. Goodenough, *Phys. Rev. B* **73** (2006) 104408.

21. H. Wu, *Phys. Rev. B* **64** (2001) 125126.

22. R.A. de Groot, F.M. Müller, P.G. van Engen, K.H.J. Buschow, *Phys. Rev. Lett*. **50** (1983) 2024.

23. J.M.D. Coey, C.L. Chien, *MRS Bull*. **28** (2003) 720.

24. A. Maignan, B. Raveau, C. Martin, M. Hervieu, *J. Solid State Chem*. **144** (1999) 224.

25. J.A. Alonso, M.T. Casais, J. Martínes-Lope, J.L. Martínes, P. Velasco, A. Muños, M.T. Fernanández-Díaz, *Chem. Mater*. **12** (2000) 161.

26. R. Rodriguez, A. Fernandez, A. Isalgue, J. Rodriguez, A. Labarta, J. Tejada, X. Obradors, *J. Phys. C: Solid State Phys.* **18** (1985) L401.

27. P.D. Battle, T.C. Gibb, A.J. Herod, S.-H. Kim, P.H. Munns, *J. Mater. Chem*. **5** (1995) 865.

28. E.J. Cussen, J.F. Vente, P.D. Battle, T.C. Gibb, *J. Mater. Chem.* **7** (1997) 459.

29. A.K. Azad, S.G. Eriksson, A. Mellergård, S.A. Ivanov, J. Eriksen, H. Rundlöf, *Mater. Res. Bull.* **37** (2002) 1797.

30. F. Millange, V. Caignaert, B. Domengès, B. Raveau, E. Suard, *Chem. Mater*. **10** (1998) 974.

31. T. Nakajima, H. Kageyama, Y. Ueda, *J. Phys. Chem. Solids* **63** (2002) 913.

32. D. Akahoshi and Y. Ueda, *J. Solid State Chem*. **156** (2001) 355.

33. J. Lindén, P. Karen, A. Kjekshus, J. Miettinen, T. Pietari, M. Karppinen, *Phys. Rev. B* **60** (1999) 15251.

34. V.P.S. Awana, J. Nakamura, J. Lindén, M. Karppinen, H. Yamauchi, *Solid. State Commun*. **119** (2001) 159.

35. J.-H. Kim, L. Mogni, F. Prado, A. Caneiro, J.A Alonso, A. Manthiram, *J. Electrochem. Soc*. **156** (2009) B1376.

36. J.-H. Kim, Y. Kim, P.A. Connor, J.T.S. Irvine, J. Bae, W. Zhou, *J. Power Sources* **194** (2009) 704.

37. M. Jin, X. Zhang, Y. Qiu, J. Sheng, *J. Alloys Compd.* **494** (2010) 359.

38. L. Zhao, B. He, B. Lin, H. Ding, S. Wang, Y. Ling, R. Peng, G. Meng, X. Liu. *J. Power Sources* **194** (2009) 835.

39. C. Zhu, X. Liu, C. Yi, L. Pei, D. Wang, D. Yan, K. Yao, T. Lue, W. Su, *J. Power Sources* **195** (2010) 3504.

40. P.M. Woodward, *Acta Cryst.* **B53** (1997) 44.

41. M.W. Lufaso, P.M. Woodward, *Acta Cryst.* **B60** (2004) 10.

42. C.J. Howard, B.J. Kennedy, P.M. Woodward, *Acta Cryst. B* **59** (2003) 463.

43. C. J. Howard, Z. Zhang, *J. Phys. Cond. Matter*, **15** (2003) 4543.

44. E.J. Williams, *Proc. Roy. Soc. London*, **152A** (1935) 231.

45. J. Rodríguez-Carvajal, *Physica B*, **192** (1993) 55.

46. H.M. Rietveld, *Acta Cryst.* **22** (1967) 151.

47. *The Rietveld Method*, IUCr Monographs on Crystallography 5, Ed. R.A. Young, Oxford University Press, New York 1993.

48. M.W. Lufaso, P.M. Woodward, *Acta Cryst. B* **57** (2001) 725.

49. K.E. Stitzer, M.D. Smith, H.-C. zur Loye, *Solid State. Sci.* **4** (2002) 311.

50. P. M. Woodward, R.-D. Hoffmann, A.W. Sleight, *J. Mater. Res.* **9** (1994) 2118.

51. B.C. Tofield, W.R. Scott, *J. Solid State Chem.* **10** (1974) 183.

52. M. K. Wu, J. R. Ashburn, C. J. Torng, P. H. Hor, R. L. Meng, L. Gao, Z. J. Huang, Y. Q. Wang, C. W. Chu, *Phys. Rev. Lett.* **58** (1987) 908.

53. M. Karppinen, H. Yamauchi, *Chemical Design of copper-oxide superconductors: Homologous Series and Oxygen Engineering* in Frontiers in Superconducting Materials, Springer Verlag 2004.

54. A. Deschanvres, B. Raveau, F. Tollemer, *Bull. Soc. Chem. Fr.* **1967** (1967) 4077.

55. Z. Zeng, M. Greenblatt, J. Sundstrom, *J. Solid State Chem.* **147** (1999) 185.

56. M. Marezio, P.D. Dernier, J. Chenavas, J.C. Joubert, *J Solid State Chem.* **6** (1973) 16.

57. N. Imamura, M. Karppinen, T. Motohashi, D. Fu, M. Itoh, H. Yamauchi, *J. Am. Chem. Soc.* **130** (2008) 14948.

58. J.A. Enterkin, P.A Maggard, S. Ishiwata, L.D. Marks, K. Poeppelmeier, M. Azuma, M. Takano, *J. Solid State Chem.* **183** (2010) 551.

59. M.C. Knapp, P.M. Woodward, *J. Solid State Chem.* **179** (2006) 1076.

60. G. King, S. Thimmaiah, A. Dwivedi, P.M. Woodward, *Chem. Mater.* **19** (2007) 6451.

61. T. Nakamura, K. Kunihara, Y. Hirose, *Mater. Res. Bull.* **16** (1981) 321.

62. T. Wada, N. Suzuki, H. Yamauchi, S. Tanaka, A. Maeda, K. Uchinokura. *J. Am. Ceram. Soc.* **72** (1989) 2000.

63. T. Nakajima, M. Ichihara, Y. Ueda, *J. Phys. Soc. Jpn.* **74** (2005) 1572.

64. T. Nakajima, H. Kageyama, Y. Ueda, *J. Phys. Chem. Solids* **63** (2002) 913.

65. T. Nakajima, H. Kageyama, H. Yoshizawa, Y. Ueda, *J. Phys. Soc. Jpn.* **71** (2002) 2843.

66. M. Karppinen, H. Okamoto, H. Fjellvåg, T. Motohashi, H. Yamauchi, *J. Solid State Chem*. **177** (2004) 2122.

67. M. Karppinen, H. Yamauchi, *Mater. Sci. Eng*. **26** (1999) 51.

68. Y.-H. Huang, J. Lindén, H. Yamauchi, M. Karppinen, *Chem. Mater*. **16** (2004) 4337.

69. K. Tezuka, K. Henmi, Y. Hinatsu, N.M. Masaki, *J. Solid State Chem*. **154** (2000) 591.

70. S. Tao, J. Canales-Vázquez, J.T.S. Irvine, *Chem. Mater*. **16** (2004) 2309.

71. N. Kashima, N. K. Inoue, T. Wada, Y. Yamaguchi, *Appl. Phys. A* **74** (2002) S805.

72. S.H. Byeon, G. Demazeau, J.-H. Choy, L. Fournes, *Mater. Lett*. **12** (1991) 163.

73. S.H. Byeon, T. Nakamura, M. Itoh, M. Matsuo, *Mater. Res. Bull*. **27** (1992) 1065-1072.

74. R.D. Shannon, *Acta Cryst. A* **32** (1976) 751.

75. J. Janicki, A. Maryanowska, J. Pietrzak, J. Suwalski, *Acta Phys. Pol*. A **68** (1985) 425.

76. A. Maryanowska, J. Pietrzak, M. Jurczyk, A. Wrzeciono, *Acta Phys. Pol. A* **72** (1987) 335-337.

77. T. Shimada, J. Nakamura, T. Motohashi, H. Yamauchi, M. Karppinen, *Chem. Mater*. **15** (2003) 4494.

78. P. Karen, *J. Solid State Chem*. **177** (2004) 281.

79. V. Pralong, V. Caignaert, S. Hebert, A. Maignan, B. Raveau, *Solid State Ionics* **177** (2006) 1879.

80. J. Seddon, E. Suard, M.A. Hayward, *J. Am. Chem. Soc*. **132** (2010) 2802.

81. C. Frontera, A. Caineiro, A.E. Carrillo, J.Oró-Solé, J.L. García-Muños, *Chem. Mater*. **17** (2005) 5439.

82. Yu.P. Chernenkov, V.P. Plakhty, V.I. Fedorov, S.N. Barilo, S.V. Shiryaev, G.L. Bychkov, *Phys. Rev. B* **71** (2005) 184105.

83. D.D. Khalyavin, D.N. Argyriou, U. Amann, A.A. Yaremchenko, V.V. Kharton, *Phys. Rev. B* **75** (2007) 134407.

84. J.-E. Jørgensen and L. Keller, *Phys. Rev. B* **77** (2008) 024427.

85. C. Frontera, J.L. García-Muños, O. Castaño, C. Ritter, A. Caineiro, *J. Phys.: Condes. Matter* **20** (2008) 104228.

86. K. Conder, E. Pomjakushina, V. Pomjakushin, M. Stingaciu, S. Streule, A. Podlesnyak, *J. Phys*.:*Condens. Matter* **17** (2005) 5813.

87. V. Caignaert, F. Millange, B. Domengès, B. Raveau, *Chem. Mater*. **11** (1999) 930.

88. E. Castillo-Martíneza, A. J. Williams, J.P. Attfield, *J. Solid State Chem*. **179** (2006) 3505.

89. C. Perca, L. Pinsard-Gaudart, A. Daoud-Aladine, M.T. Fernández-Díaz, J. Rodríguez-Carvajal, *Chem. Mater*. **17** (2005) 1835.

90. K. Ramesha, J. Gopalakrishnan, V. Smolyaninova, R.L. Greene, *J. Solid State Chem.* **162** (2001) 250.

91. T. K. Mandal, A. M. Abakumov, M. V. Lobanov, M. Croft, V. V. Poltavets, M. Greenblatt, *Chem. Mater.* **20** (2008) 4653.

92. C. Frontera, D. Rubí, J. Navarro, J.L. García-Muños, C. Ritter, J. Fonctuberta, *Physica B* **250** (2004) E285.

93. D. Sánchez, J.A. Alonso, M. García-Hernández, M.J. Martínez-Lope, M.T. Casais, J.L. Martínez, M.T. Fernández-Díaz, *J. Magn.Magn. Mater*. **272–276** (2004) 1732.

94. J. Lindén, T. Shimada, T. Motohashi, H. Yamauchi, M. Karppinen, *Solid State Commun*. 129 (2004) 129.

95. M. Karppinen, H. Yamauchi, Y. Yasukawa. J. Lindén, T.S. Chan, R.S. Liu, J.M. Chen, *Chem. Mater*. **15** (2003) 4118.

96. Md. Motin Seikh, Ch. Simon, V. Caignaert, V. Pralong, M. B. Lepetit, S. Boudin, B. Raveau, *Chem. Mater*. **20** (2008) 231.

97. K. Fujinami, M. Karppinen, H. Yamauchi, *Physica C* **300** (1998) 17.

98. M. Karppinen, H. Yamauchi, T. Nakane, K. Fujinami, K. Lehmus, P. Nachimuthu, R.S. Liu, J.M. Chen, *J. Solid State Chem*. **166** (2002) 229.

99. M. Karppinen, H. Yamauchi, K. Fujinami, T. Nakane, K. Peitola, H. Rundlöf, R. Tellgren, *Phys. Rev. B* **60** (1999) 4378.

100. Y.-H. Huang, R.I. Dass, Z.-L. Xing, J.B. Goodenough, *Science* **312** (2006) 257.

101. C. Bernuy-Lopez, M. Allix, C. A. Bridges, J. B. Claridge, M. J. Rosseinsky, *Chem. Mater*. **19** (2007) 1035.

102. S. Vasala, M. Lehtimäki, Y.H. Huang, H. Yamauchi, J.B. Goodenough, M. Karppinen, *J. Solid State Chem.* 2010, *in press.*

103. F. Sher, A. Venimadhav, M.G. Blamire, K. Kamenev, J.P. Attfield, *Chem. Mater*. **17** (2005) 176.

104. M. Karppinen, M. Matvejeff, K. Salomäki, H. Yamauchi, *J. Mater. Chem*. **12** (2002), 1761.

105. M. Karppinen, A. Fukuoka, L. Niinistö, H. Yamauchi, *Supercond. Sci. Technol*. **9** (1996) 121.

106. M. Matvejeff, M. Lehtimäki, A. Hirasa, Y.-H. Huang, H. Yamauchi, M. Karppinen, *Chem. Mater*. **17** (2005) 2775.

107. N.N. Greenwood and T.C. Gibbs, *Mössbauer Spectroscopy*, Chapman and Hall Ltd., London 1971.

108. J.-S. Kang, J.H. Kim, A. Sekiyama, S. Kasai, S. Suga, S.W. Han, K.H. Kim, T. Muro, Y. Saitoh, C. Hwang, C.G. Olson, B.J. Park, B.W. Lee, J.H. Shim, J.H. Park, B.I. Min, *Phys. Rev. B* **66** (2002) 113105.

109. J.P. Crocombette, M. Pollak, F. Jollet, N. Thromat, M. Gautier-Soyer, *Phys. Rev. B* **52** (1995) 3143.

110. A.M. Glazer, *Acta Cryst. B* **28** (1972) 3384.

111. T. Nakajima, H. Kageyama, Y. Ueda, *J. Magn. Magn. Mater*. **272-267** (2004) 405.

112. F. Fauth, E. Suard, V. Caignaert, *Phys. Rev. B* **65** (2001) 60401.

113. A.K. Kundu, E.-L. Rautama, Ph. Boullay, V. Caignaert, V. Pralong, B. Raveau, *Phys. Rev. B* **76** (2007) 184432.

114. F. Fauth, E. Suard, V. Caignaert, I. Mirebau, *Phys. Rev. B* **66** (2002) 184421.

115. V.P. Plakhty, Yu.P. Chernenkov, S.N. Barilo, A. Podlesnyak, E. Pomjakushina, E.V. Moskvin, S.V. Gavrilov, *Phys. Rev. B* **71** (2005) 214407.

116. C. Kittel, *Introduction to Solid State Physics*, 6th Ed., John Wiley & Sons Inc., New York 1986.

117. S.B. Kim, B.W. Lee, C.S. Kim, *J. Magn. Magn. Mater*. **242-245** (2002) 747.

118. S. Elliot, *The Physics and Chemistry of Solids*, 2nd Ed., John Wiley & Sons, Great Britain 2000, p. 728.

119. P. Hohenberg, W. Kohn, *Phys. Rev.* **136** (1964) B864.

120. W. Kohn, L.J. Sham, *Phys. Rev*. **140** (1965) A1133.

121. V. Anisimov, J. Zaanen, O.K. Andersen, *Phys. Rev. B* **44** (1991) 943.

122. V. Anisimov, I.V. Solovyev, M.A. Korotin, M.T. Czyzk, G.A. Sawatzky, *Phys. Rev. B* **48** (1993) 16929.

123. U. von Barth, L. Hedin, *J. Phys. C* **5** (1972) 1629.

124. N. Hamada, private communication.

125. I. Solovyev, N. Hamada, K. Terakura, *Phys. Rev. B* **53** (1996) 7158.

126. O.K. Andersen, *Phys. Rev. B* **12** (1975) 3060.

127. Y. Moritomo, Sh. Xu, T. Akimoto, A. Machida, N. Hamada, K. Ohoyama, E. Nishibori, M. Takata, M. Sakata, *Phys. Rev. B* **62** (2000) 14224.

128. J. C. Burley, J. F. Mitchell, S. Short, D. Milelr, Y. Tang*, J. Solid State Chem*. **170** (2003) 339.

129. P.S. Anderson, C.A. Kirk, J. Knudsen, I.M. Reaney, A.R. West, *Solid State Sci*. **7** (2005) 1149.

130. Md M. Seikh, V. Caignaert, V. Pralong, Ch. Simon, B. Raveau, *J. Phys.: Condens. Matter* **20** (2008) 015212.

131. M. Respaud, C. Frontera, J.L. García-Muñoz, M.A.G. Aranda, B. Raquet, J.M. Broto, H. Rakoto, M. Goiran, A. Llobet, J. Rodríguez-Carvajal, *Phys. Rev. B* **64** (2001) 214401.

132. H.D. Zhou, J.B. Goodenough, *J. Solid State Chem*. **177** (2004) 3339.

133. C. Frontera, J.L. García-Muños, A.E. Carillo, M.A.G. Aranda, I. Margiolaki, A. Caneiro, *Phys. Rev. B* **74** (2006) 054406.